HIGH-FREQUENCY MOTION RESIDUALS IN MULTIBEAM ECHOSOUNDER DATA: ANALYSIS AND ESTIMATION

BY

BRANDON MAINGOT
B.S. in Geomatics Engineering, University of the West Indies, 2014

THESIS

Submitted to the University of New Hampshire
in Partial Fulfillment of
the Requirements for the Degree of

Master of Science
in
Ocean Engineering: Ocean Mapping

September 2019

This thesis was examined and approved in the partial fulfillment of the requirements for the degree of Master of Science in Ocean Engineering: Ocean Mapping by:

Thesis Director, John Hughes Clarke, Professor of Ocean Engineering, and Earth Sciences

Brian Calder, Research Professor of Ocean Engineering

Giuseppe Masetti, Research Assistant Professor of Ocean Engineering

On July 30th ,2019

Approval signatures are on file with the University of New Hampshire Graduate School.

ACKNOWLEDGEMENTS

My heartfelt thanks go out to my family, friends and teachers, particularly my defense committee and advisor, John. They have inspired many of the ideas presented in this thesis, and my pursuit of them.

TABLE OF CONTENTS

ABSTRACT

HIGH-FREQUENCY MOTION RESIDUALS IN MULTIBEAM ECHOSOUNDER DATA: ANALYSIS AND ESTIMATION

by

Brandon Maingot

University of New Hampshire

Advances in multibeam sonar mapping and data visualization have increasingly brought to light the subtle integration errors remaining in bathymetric datasets. Traditional field calibration procedures, such as the patch test, just account for static orientation bias and sonar-to-position latency. This, however, ignores the generally subtler integration problems that generate time-varying depth errors.

Such dynamic depth errors are the result of an unknown offset in one or more of orientation, space, sound speed or time between the sonar and ancillary sensors. Such errors are systematic, and thus should be predictable, based on their relationship between the input data and integrated output. A first attempt at addressing this problem utilized correlations between motion and temporally smoothed, ping-averaged residuals. The known limitations of that approach, however, included only being able to estimate the dominant integration error, imperfectly accounting for irregularly spaced sounding distribution and only working in shallow water.

This thesis presents a new and improved means of considering the dynamics of the integration error signatures which can address multiple issues simultaneously, better account for along-track sounding distribution, and is not restricted to shallow water geometry. The motion-driven signatures of six common errors are simultaneously identified. This is achieved through individually considering each sounding's input-error relationship along extended sections of a single swath corridor. Such an approach provides a means of underway system optimization using nothing more than the bathymetry of typical seafloors acquired during transit. Initial results of the new algorithm are presented using data generated from a simulator, with known inputs and integration errors, to test the efficacy of the method. Results indicate that successful estimation requires conditions of significant vessel motion over periods of a few tens of seconds as well as smooth, gently rolling bathymetry along the equivalent spatial extent covered by the moving survey platform.

I – INTRODUCTION

1.1 – Motivation and Overview

Multibeam bathymetric mapping, a marine acoustic remote sensing technique, requires the integration of platform orientation and position measurements, along with array-relative ranges and angles, in order to georeference – that is, model the location of – remote seafloor interactions. While individual sensors may be calibrated, by their manufacturers for example, their offsets in space, orientation and time, relative to the sonar, are often difficult to measure when installed separately on that platform [1]. Those integration parameters beyond the core set estimated by the patch test are typically ignored, as their influence on the final solution is usually just within the allowable total accuracy limits. While small, however, these errors often are present in bathymetry [2], propagating as high-frequency, motion dependent depth errors (Fig. 1).

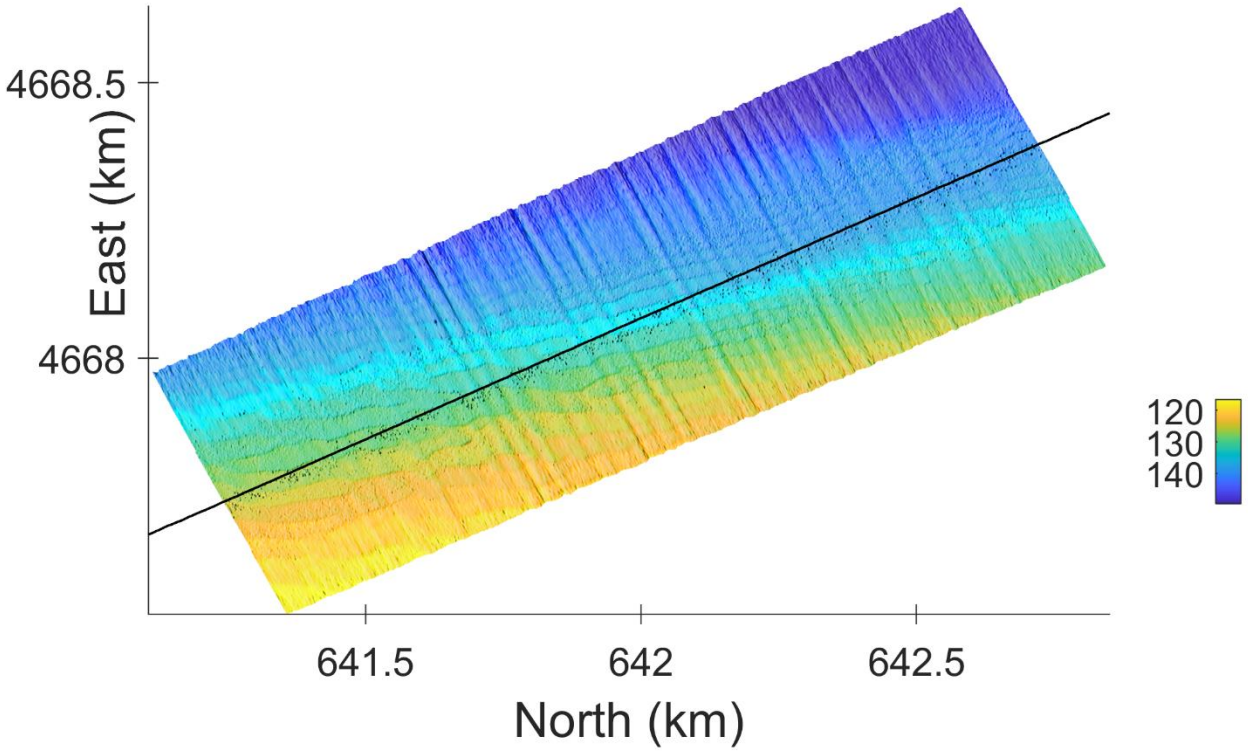

Figure 1: Sun-illuminated bathymetry, acquired in approximately 130m of water, containing wobble due to an unknown error. The artificial signature, oriented transverse to the ship track, is notably of similar scale and wavelength to that of the fine detail bed-forms also present in the image, though approximately parallel to ship track here. Such artificial signatures can significantly obstruct the analysis of fine-scale relief, particularly if unfortunate enough to be parallel to the superimposed artefact. Data courtesy of NOAA Ship Thomas Jefferson. Results are projected in UTM zone 20.

The technological advance in sensors and visualization since the introduction of multibeam systems has brought to light the increasingly subtle imperfections in system integration causing errors now greater than achievable feature resolution ([2], [3]) (Fig. 1). This advancement in sensor precision and accuracy has enabled the resolution of features as fine as 0.1-0.2% water depth in height over length scales of approximately 3% water depth [3].

Coastal and ocean environments worldwide are coming under increasing pressure regarding resource development, and many maritime countries are recognizing that much higher resolution bathymetric data are needed for sustainable management of offshore resources [4]. For over two

decades, high frequency multibeam echo-sounders (MBES) have been recognized as a powerful means of investigating shallow water seafloor processes and coastal zone characterization and delimitation, among other applications ([5], [6], [7], [8], [9]). High resolution sonars are limited by their sensor noise floor. To adequately identify the fine detail features often sought for these applications, systematic errors which result in depth errors greater the smallest resolvable vertical scale must be corrected for ([2], [5]). As the cost of the technology has reduced, it is now cost-effective to image large areas of the seafloor in coastal regions to provide baseline data for planning [8], and accurate integration of the ever-increasingly rapid acquisition of bathymetry is desired for its best use.

1.2 – Constraints and Challenges

To adequately quantify these integration errors, an error estimation algorithm must account for:

1. Irregular spacing in seafloor sampling: A vessel in dynamic motion inherently samples a corridor of the seafloor in an irregular manner. The advent of multi-sector active motion compensation enhances the coverage of the seafloor through appropriately steering sectors of swath along track. Each sector's transmission, modelled as a cone leaving the transmitter, is steered along-track with a unique angle. Combining the multiple the sequentially emitted cones' intersection with the seafloor into a single across-track swath, adds complexity to the soundings' spatial distribution.
2. Time evolution of the error signature: The signature of the errors are primarily functions of vessel orientation, rate of angular motion and heave. As such, the error projected on the seafloor oscillates with a wavelength equal to the product of vessel speed and the characteristic ocean wave period. The realized errors thus evolve over consecutive pings in shallow water, defines as depths where the shot-receive cycle of pings are short

relative to the wave-driven vessel oscillation period. This sees the error eventually evolving over adjacent beams as depth increases, complicating analysis at depth.

3. Unknown bathymetric truth: The "true", or rather higher accuracy estimate, of the underlying seafloor is typically unknown in pioneering ocean mapping missions. Further, unless the area has been previously surveyed with a system free of integration error or with means of producing higher accuracy products, existing data may not be suitable for analysis. To make this method work opportunistically, an estimate of the true seafloor needs to be derived from the imperfect underway swath corridor itself.
4. Seafloor tilt and curvature: Much of the seafloor has natural slope and long wavelength curvature to it. Compounded with irregular sampling of the seafloor, this results in irregular depth variation between adjacent pings and, at times, even beams. Trend removal is required to account for this, while not fitting the oscillation of wobbles. Separating low frequency seafloor trends from the relatively high frequency projected wobble is demonstrably feasible [2]. It does, however, require considering extended seafloor extents, such as four wave periods, if only using bathymetry acquired in situ [2]. Seafloor complexity is likely to evolve over extended spatial extents, however, and simple trends may thus become increasingly poor estimates of the underlying seafloor, and, therefore a balance must be found.
5. True seafloor roughness: Dynamic motion residuals add an artificial "roughness" to bathymetric data, which can be difficult to discern from real seafloor roughness, such as rock outcrops and sand ripples. There is a need for recognizing natural rugosity.
6. Multiple error sources: There is an overarching need to ensure every parameter within the regression model has a uniquely identifiable depth signature. This is a result of regression

minimizing errors as a function of the defined parameters. Some integration errors share similar relationships between the dynamic depth errors and their drivers, making them difficult to distinguish under non-ideal conditions, such as insignificant or identical angular component motions, predominantly roll and pitch. Further, any depth variations not accounted for by the seafloor and sounding model, unless entirely independent of the integration errors and their combinations, are absorbed into their regression estimates.

7. Spurious bottom detections and pings: Across track profiles with spurious bottom detections can severely degrade regression estimates. Particularly when applying least squares approaches to small datasets, a need to compensate for outlier measures arises outside of a simulated environment, such as CUBE [10].

Imperfect accounting for 1) irregular seafloor sampling, 2) time evolution of the propagated depth error, and 4) seafloor tilt and curvature were the main limitations of the method of [2]. This thesis seeks to address these deficiencies and extend the approach of [2] to produce a calibration which can be used more generally. Specifically, for the calibration to operate in all water depths and in the presence of multiple error sources, while better accounting for sounding distribution.

1.3 – Proposed Approach

There are four main components to this research:

1) development of a georeference equation in which all the integration errors are defined as parameters,
2) development of a sounding distribution simulator,
3) derivation of a suitable reference surface for the true seafloor,

4) optimization of, as a function of the integration errors, a “wobbled” synthetic swath corridor against the reference surface, which is simultaneously derived. Estimates are then compared against their known, forced values.

A sounding georeference equation which contains each of the errors provides a means of coupling them to each during multivariate optimization. The result is that correlated depth signatures of various integration errors can be distinguished, which would otherwise bias estimates of the ambiguous errors. Further, provided some surface to sample, this equation enables simulation of swath corridor geometry under designed input. That input includes various characteristic seafloor undulation wavelengths, amplitudes and azimuths, as well as magnitudes of integration error and vessel motion.

For this proof of concept, such an idealized environment is suitable for identifying the theoretical capability of the proposed method, in both estimating the true underlying seafloor, and more critically, the desired integration errors. Analyses are carried out simulating various input setups and conditions, chosen to crudely represent environmental conditions, in order to assess the method’s robustness. Proven successful with simulated data, a future intention, though beyond the scope of this Master’s thesis, is to implement this on field data.

1.3.1 – Rigorous Inter-Sensor Calibrator (RISC)

The error extraction model is designed considering the short and long wavelength nature of respectively the propagated errors and seafloor undulation. The “wobbled” soundings are flattened to an ideally smooth, long wavelength seafloor, as simultaneously approximated by a quadratic surface. This is done through equating the two models, using the same sounding as the depth observation for each:

$$\Delta z = (z_s - \epsilon_s) - \left(z_q - \epsilon_q\right) = f(\mathbf{x}_s, \boldsymbol{\beta}_s) - g\left(\mathbf{x}_q, \boldsymbol{\beta}_q\right),$$

$$\Delta z = (z_s(\mathbf{x}_s, \boldsymbol{\beta}_s) - \epsilon_s) - \left(z_s(\mathbf{x}_s, \boldsymbol{\beta}_s) - \epsilon_q\right) = f(\mathbf{x}_s, \boldsymbol{\beta}_s) - g\left(\mathbf{x}_q, \boldsymbol{\beta}_q\right),$$

$$\Delta z = \epsilon_q - \epsilon_s = f(\mathbf{x}_s, \boldsymbol{\beta}_s) - g\left(\mathbf{x}_q, \boldsymbol{\beta}_q\right),$$

$$\Delta z = \epsilon = h(\mathbf{x}, \boldsymbol{\beta}).$$

Thus the residuals of the combined model to be optimized are attributed to the disturbances, or signatures, unaccounted for by both the sounding location and parametric surface models. Solving both models simultaneously accounts for potential correlations among the integration errors and seafloor trends. The model ideally equals zero for all observations.

The multitude of soundings acquired by swath systems implies the system becomes overdetermined after a few pings of measurements. The system may then be optimized through minimizing the sum of squares. The sounding location component of $h(\boldsymbol{X}, \boldsymbol{\beta})$**,** described in the following section, is nonlinear in the integration errors, subsequently, so are the first order conditions used to determine the minimum in optimization [11]. The six integration errors are detailed in Chapter 2.2. Generally**,** no simple closed form solution for the conditions exists [11] and a numerical nonlinear regression technique is then required to optimize the system's L2-norm. For this preliminary study of the method's validity, a simple Gauss-Newton approach [12] is taken to optimize this nonlinear least squares problem.

The calibration procedure considers a continuous swath of data and, through a generalized moving average approach, estimates smoothed measures of the seafloor trends and each of the designed integration errors (Fig. 2). The cumulative average of these smoothed estimates is expected to asymptotically converge to truth in non-pathological combinations of vessel motion and seafloor relief. This is explored using characteristic wave periods and wavelengths in Chapter 4. Thus the method acts as an effective calibrator of inter-sensor offsets, capable of

continuously monitoring and updating cumulative averages of each as more data is acquired. This requires no prior knowledge of bathymetry, simply that the assumption of smooth, long wavelength curvature is upheld.

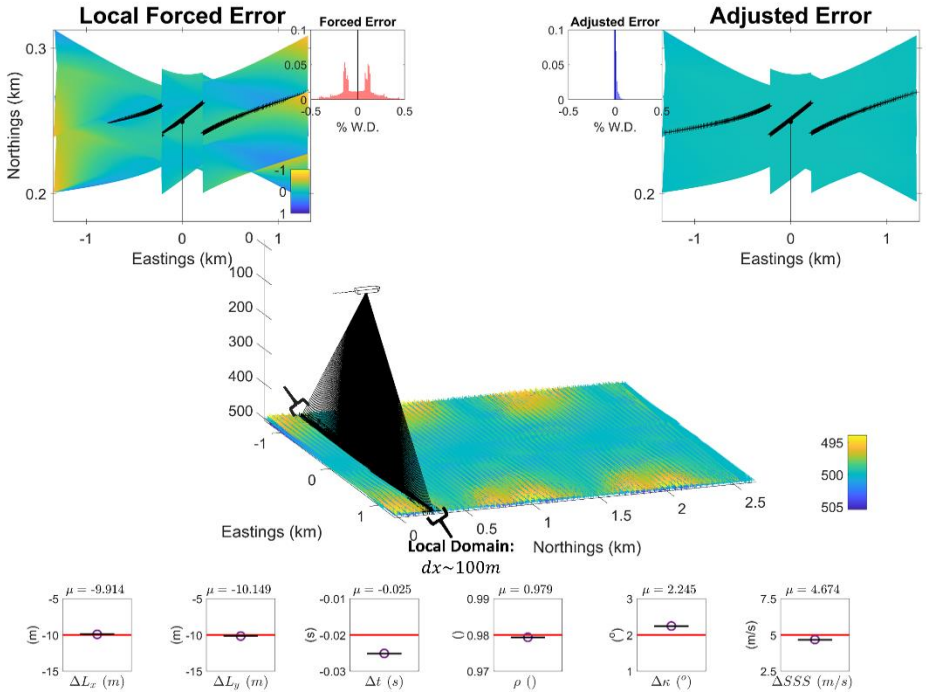

Figure 2: Illustration of RISC operating on a subsection of swath corridor (middle, black crosses), simultaneous filtering the seafloor with a 2D quadratic and estimating the remaining wobble using the designed integration errors (bottom row, true values in red). Local estimates are made for each error (bottom row, purple circles) which are combined into a regional estimate (bottom row, black lines, number of local estimates =1). The vessel is steaming directly north, and parameters are continuously estimated using the local residuals (raw residuals top left, adjusted residuals top right, black crosses represent a single ping).

Considering the sonar system's bottom tracking standard deviation to be at best around 0.1-0.2% water depth [3], calibration is here deemed sufficient when bias in asymptotic averages reduces to magnitudes resulting in propagated depth errors < 0.1% water depth. The primary goal of this thesis is to achieve this in all water depths. While combinations of vessel motion and seafloor relief ideal for estimating the offsets reliably are not expected to be continuously present, they are expected to arise to a satisfactory extent in the abundant swath corridor datasets typically acquired for survey operations. By computing the asymptotic average, more information useful in discriminating the correlated parameters is added to the system. Field implementation should

omit spurious estimates from the cumulative running average through manual data cleaning, though more sophisticated approaches of asserting solution reliability are recommended for future work.

1.3.2 – An Analytical, Wobble-Compensating, Swath System Integration

An equation is developed which georeferences soundings based on the raw observations acquired by a sonar system suite. A global navigational satellite system (GNSS) receiver measures positions within a larger coordinate system, WGS84, which are typically projected to a mapping reference frame (MRF), such as Universal Transverse Mercator (UTM), in which the array-relative measures are then georeferenced. The integration model of the sensor suite's datasets must be a continuously differentiable (C^1) function of the integration errors in order for calibration through optimization to be possible [11]. A result of the depth-varying sound speed of the water through which the emitted sound travels, is that a numerical ray trace through depth-discretized layers is required for accurate georeferencing. Thus, after determining the transmission's initial geographic vector, here using a concentric, non-orthogonal cone-cone intersection, such as seen in [13], a typical time based, curvilinear ray trace procedure [14] is done and two new variables are calculated:

1) s, the linear slant range from the signal's origin to the georeferenced sounding,
2) ϕ_R, the angular deflection from the transmitted departure due to refraction.

These variables are then integrated with the initial, generic vector representation of the transmission, to produce a final georeference equation which equivalently represents the integrated sounding solution (Fig. 3) in a continuously differentiable form:

$$\mathbf{X}_s = \mathbf{MB}^{\mathrm{MRF}} + s \cdot \begin{bmatrix} \cos(\phi + \phi_R)\cos\theta \\ \cos(\phi + \phi_R)\sin\theta \\ \sin(\phi + \phi_R) \end{bmatrix},$$

where:

- $\mathbf{X}_s =$ Sounding coordinate,
- $\mathbf{MB}^{\mathrm{MRF}} =$ Average MBES location between shot and reception of signal, in MRF,
- $\phi =$ Depression angle of signal relative to water line, or local level,
- $\theta =$ Azimuth of signal relative to North.

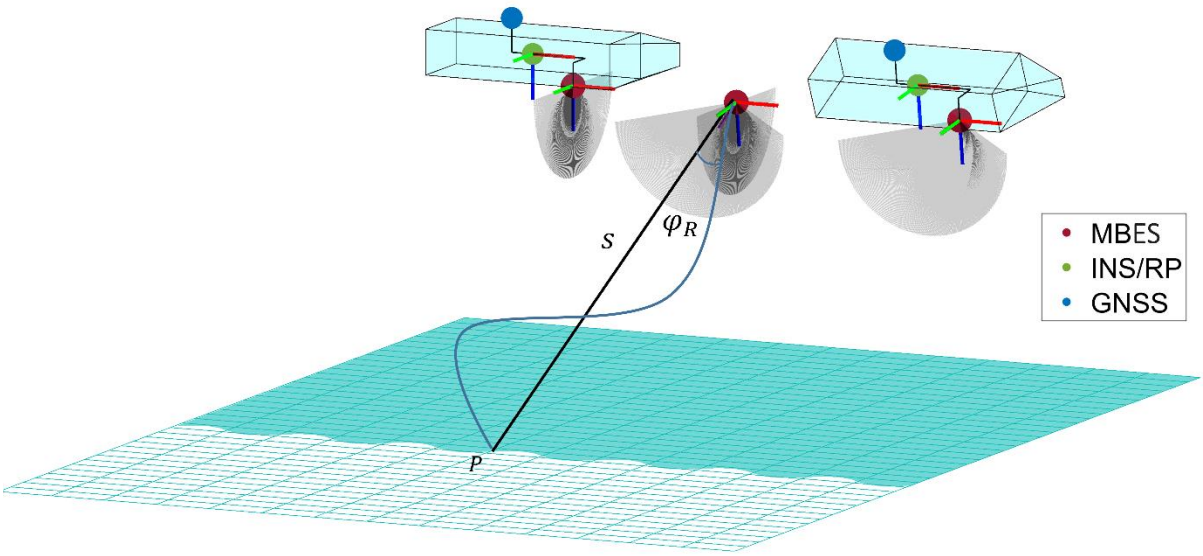

Figure 3: The geometric components of the analytical concentric integration model implemented in this thesis. An along-track transmit angle and across-track receive angle are combined for a virtual reference frame, centered at $\boldsymbol{MB}^{MRF}$. A simulated swath corridor in solid green is overlain the "true" simulated seafloor in green mesh. Separation between the signal's transmission and reception is grossly exaggerated for illustration.

The errors exist within the equation as systematic components, and are here treated as parameters. In theory, every observation has a systematic and stochastic component, the latter of which contains measurement errors and the combination of all signals not adequately accounted for by the model [15, 16] [16]. For real data, the number of contributing error sources is high,

and the total resulting errors are approximately Gaussian distributed [16]. These errors ideally combine to produce a random signal. A statistical expression for a single depth observation of the georeference equation is then:

$$z_s = \mathbf{MB}^{\mathbf{MRF}}(z) + s \cdot \sin(\phi + \phi_R) + \epsilon_s$$
$$= f(\mathbf{x}_s, \boldsymbol{\beta}_s) + \epsilon_s$$

where:

- $z_s =$ Sounding depth,
- $\boldsymbol{\beta}_s =$ Vector of integration errors (parameters),
- $\mathbf{x}_s =$ Vector of auxiliary sensor input (variables),
- $\epsilon_s =$ Sounding depth disturbance (true error).

1.3.3 – Simulation of Spatial Sounding and Error Distributions

A swath simulator was developed to produce swath corridor datasets under input conditions characteristic of ocean environments and containing known integration errors. Data analysis focuses on the impact of the combination the survey platform's component angular velocities and phase offsets, in addition to seafloor depth and undulation wavelength. These are the bathymetric errors' primary driving signatures. Spatially parametrizing the seafloor as a two-dimensional sinusoid and temporally parametrizing angular vessel motion and heave as sinusoids provides a simple means of creating a variety of conditions useful for identifying the capability and robustness of the proposed method. Such parameterization enables the calculation of the resulting two-way travel time (TWTT) to be made from an exactly known origin to an exactly known point on the seafloor, using what is referred to herein as an "inverse" ray trace procedure.

Through specifying multibeam configurations of swath width, stabilization strategies, number of sectors and beams, and ping rate, the remaining time and space-varying inputs to the system can be set through evaluating their corresponding parameterizations to produce a swath corridor of beam vector-seafloor intersections. These are assigned as soundings. Figure 2 illustrates the surface realization of such a simulated corridor. Each inverse ray trace calculates a TWTT, which is then reintegrated with errors forced onto the input parameterizations using a forward ray trace in order to produce the corresponding "wobbled" dataset. These datasets are analyzed in Chapter 4 to assess the proposed method's ability to simultaneously estimate the forced, and therefore known, integration errors.

1.3.4 – Detrending the Seafloor, Extracting the Wobble

A consequence of many ocean mapping endeavors being pioneering work is that datasets are acquired over areas where high accuracy reference surfaces are yet to be established. Faced with only a growing corridor of imperfectly integrated soundings, in order to calculate those imperfections, an estimate of the true seafloor is nonetheless needed.

To identify false undulations due to integration errors, seafloors with only spatial wavelengths significantly longer than the projected wobbles' are desired. For example, wobbles are projected on the seafloor with wavelength of approximately 40 m when a swath corridor is collected by a vessel steaming straight at 5 m/s in the presence of an 8 s ocean wave driving platform oscillation (Fig. 4). For many sedimented seafloors of the continental shelf and over abyssal plains, the assumption of long characteristic wavelength seafloor undulation is reasonable.

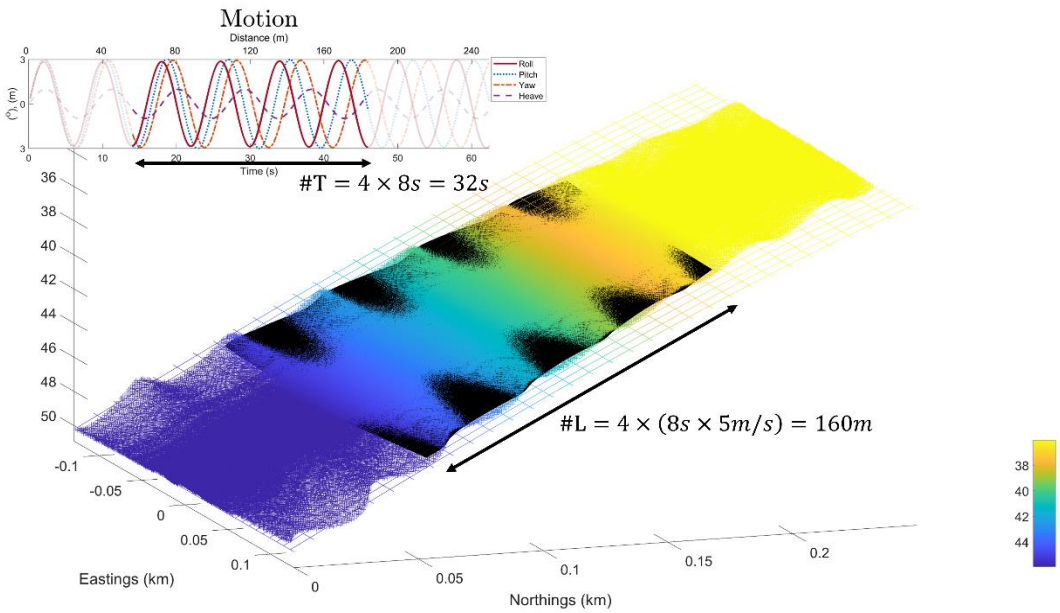

Figure 4: Swath corridor simulated with 6 simultaneous errors when driven by the motion time series illustrated top left. A subsection of wobbled swath corridor, spanning four wave periods, or 160 m (illustrated as relief-colored crosses) is used to approximate the true underlying seafloor (illustrated as a mesh).

To separate the wobbles from the assumed low frequency seafloor, a domain extent longer than that of the expected wobbles (here, 40 m) is required (Fig. 4). The method presented here seeks to extract the higher frequency wobbles from the lower frequency seafloor using only the in situ soundings, isolating the wobbles for analysis. The approach adopted is to assume the surveyed seafloor is a smooth surface that changes only over spatial scales long with respect to the integrations errors' projection onto the seafloor. A two-dimensional, quadratic model is proposed (Fig. 4):

$$z_q = \beta_0 + \beta_1 x + \beta_2 y + \beta_3 x^2 + \beta_4 y^2 + \epsilon_q,$$

$$= g(\mathbf{x}_q, \boldsymbol{\beta}_q) + \epsilon_q,$$

where:

- z_q = Quadratic surface depth at horizontal sounding coordinate (output variable),
- $\beta_{0:4}$ = Quadratic surface trends (parameters),

- $x, y =$ Estimated horizontal sounding coordinate (input variables),
- $\epsilon_q =$ Quadratic surface depth disturbance (true error).

The quadratic surface (Fig. 4, black) is naturally restricted to one inflexion along and across-track, thus "threading" the wobbled swath corridor.

Natural seafloor complexity may be identified through analyzing the variance of depth residuals relative to a regionally estimated truth [2]. This approach is recommended for identifying suitable regions of seafloor in field implementation, in a slightly augmented form more suited to the implemented quadratic fit, requiring the 90% of the depth residuals made relative to the surface to be less than 0.5% water depth. More sophisticated data selection is recommended for future work and not expanded on this thesis.

1.4 – Thesis Contributions

This thesis delivers a method which, automatically and simultaneously, quantifies common sources of high frequency depth errors. While this problem has been previously investigated [2], simplifying assumptions result in the method being effective only in minimally sloped, shallow water environments where only one error is dominant. With the increase in system precision and visualization capability, a new, more precise method is needed for calibration.

The approach developed here uniquely considers the input-error correlations for each sounding, as opposed to for each ping as done by [2]. Thus, it is applicable in all water depths, including in water sufficiently shallow that a ping's shot-receive cycle is far shorter than the wave-induced period of vessel oscillation, and thus the time-evolution of the depth error. Modified terms for multibeam orientation, position and array-relative angles that couple the integration errors are presented, as well as a means of making the ray trace component of a typical concentric

georeference model computationally tractable. This produces a georeference model which can be implemented through regression analysis and can account for the correlations among the errors, provided some ground truth. The rigorous inter-sensor calibrator, RISC, presented here, creates this reference using only the in situ soundings acquired by the swath system.

1.4.1 – Specific Deliverables

The method's implementation as a general smoothing approach, detailed in Chapter 3, is designed to be robust to the seafloor shape typical in bathymetry, as well as fleeting irregularities, such as spurious rock outcrops. The method does not require particular line geometries or overlap, thus adding no time to survey. Its implementation further enables near-real-time calculation, and thus "monitoring" of the integration errors. This sees advantage in the presence of slowly varying errors, such as surface sound speed bias, as the errors can monitored and updated as they evolve during field operations. The automatic nature of the calibration is particularly useful for autonomous systems, as errors can be rectified prior to data retrieval, ensuring data is optimally collected. This is particularly applicable to dynamic motion compensation which uses the estimated multibeam orientation to ensure optimal bottom coverage.

A swath simulator is developed as a series of equations. The simulator offers a means of investigating the propagated magnitude of depth errors under various input time and space series, and could be easily expanded to use a real digital elevation model (DEM) instead of a synthetic sinusoid as the simulation's "true" seafloor.

As an additional benefit, the uncertainty of the integration error estimates may be employed as components in the calculation of sounding TPU for implementation in automatic data cleaning

procedures. More accurate estimation of the uncertainties, however, requires more rigorous consideration of input uncertainties than pursued here.

1.5 – Outline of Thesis

This thesis first gives an overview of how the concentric georeference model is simulated in order to produce data for analysis. Next, six errors common to bathymetry [2] and the nature of their propagation from the raw auxiliary sensor input to shallow- and deep-water bathymetry are briefly discussed. A review of existing sonar calibration methods, as well as notably applicable lidar methods, follows. RISC is then presented. Finally, simulated results acquired over a seafloor modelled at various depths and wavelengths are analyzed when driven by both synthetic and real vessel motion, in order to assess the method's capability.

II –BACKGROUND

2.1 – Simulating Sounding Integration

Either a real dataset with a known set of errors or a simulated dataset is needed to assess the method's ability to estimate integration errors. Since the former does not exist, a simulator has been developed such that all conditions can be controlled, and those expected to have greatest influence on the estimates can be analyzed under conditions of interest. The simulator models a three-sector, three-axis stabilized multibeam mounted on a heaving, rolling, pitching and yawing vessel, made to steam in a straight line over an undulating seafloor (Fig. 5). This swath geometry is particularly relevant to the triple sector systems employed by much of National Oceanic and Atmospheric Administration's (NOAA) current Office of Coast Surveys (OCS) fleet. A concentric intersection of two non-orthogonal cones is used to combine the sonar's transmit and receive measures, such as that seen in [13]. All of this is implemented as a series of equations, which are used to directly compute the spatial distribution of soundings resulting from a parameterized set of input.

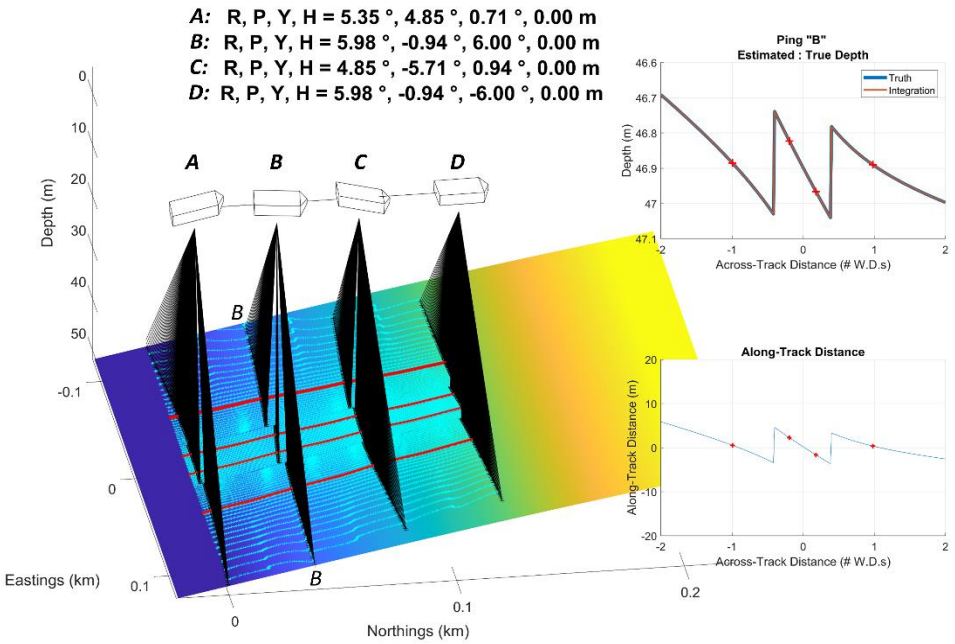

Figure 5: "Perfect" output of multi-sector swath simulator developed to test the RISC approach. Along-track discontinuities (inset, bottom) resulting from motion compensation corresponds to apparent depth discontinuities across-track (inset, top) in the presence of regional relief.

Sensor input includes:

- $\mathbf{GNSS}^{\mathrm{MRF}}$ = positions in a mapping reference frame (MRF),
- (ω, ϕ, κ) = roll, pitch, heading triplets of Tait-Bryan angles defining orientation [17],
- $(\theta_{Tx}, \theta_{Rx})$ = array-relative angles at which sound is transmitted and received,
- *SSP* = sound speed profile
- *TWTT* = two way travel time.

Each of these classes of measure, apart from TWTT, must be determined at both the epochs of signal transmission and reception for accurate integration. The TWTT is implicit to the active remote sensing procedure, and as a result, is the most difficult to calculate in simulation. The array-relative angles are defined as those required to steer the arrays' cones of sensitivities to some desired geographic angle. Every other input can be trivially parameterized for simulation,

with the seafloor, component angular motions and heave all being defined here as sinusoids to provide flexibility for analysis in Chapter 4:

$$[\omega, \phi, \kappa, Hv] = [a_1, a_2, a_3, a_4] \cdot \sin(2\pi \cdot [f_1, f_2, f_3, f_4] \cdot t + [\Phi_1, \Phi_2, \Phi_3, \Phi_4]).$$

The simulator presented here assumes across-track motion compensation to be identical to the roll of the receiver array: $\theta_{Rx}^{VRF} = \theta_{Rx}^{MRF} - \omega_{Rx}$, where θ_{Rx}^{MRF} is a discrete across-track angle defined ahead of time: for example, one of 400 beams having equiangular spacing, across a swath spanning $\pm$65° relative to the geographic vertical. A single along-track motion compensation angle must take into account both the transmitter's heading and pitch when steering each sector's transmission to a desired geographic along-track angle, θ_{Tx}^{MRF}, specified here as nadir.

An along-track steering angle, θ_{Tx}^{VRF}, is derived as that required to shift a designated across-track angle along the circumference of a cone from its "un-steered" along-track displacement (orange line, Fig. 6) to nadir (red plane, Fig. 6c). Specifying the cone with unit slant height simplifies the equation, as does steering beams to nadir since the associated terms cancel from the equation. The resulting angle, θ_{Tx}^{VRF}, is that which produces the along-track "rise" to nadir over the "run" of the cone's unit slant height. :

$$\theta_{Tx}^{VRF} = \operatorname{atan}\left(-\sin\kappa_{Tx}\sin\theta_{Rx}^{MRF} + \cos\kappa_{Tx}\sin\phi_{Tx}\left(1 - \sqrt{\sin^2\theta_{Rx}^{MRF}}\right)\right).$$

Each sector's designated angle, θ_{Rx}^{MRF} above, is specified by the multibeam's swath configuration, here defined as having three sectors with roughly the same width, geographically centered on -45°, 0°, 45°. These center angles are the sectors' designated angles, though notably apart from the central sector, which is not yaw stabilized, and pitch stabilization is based on the

15° beam instead of the midpoint for optimal coverage. The un-steered along-track displacement, or "rise", is calculated by aligning the transmitter, $\mathbf{n}_{Tx}$, and the y and z axes of an un-steered cone, which is simply a circle. The heading rotation for yaw stabilization, κ_{Tx}, is relative to the transmitter's course made good (CMG), here taken to be North, or 0°.The pitch angle is that of the transmitter, and the appropriate roll angle is implicit in the geographic, receive across-track angle, θ_{Rx}^{MRF}, making x-axis alignment of the cone unnecessary.

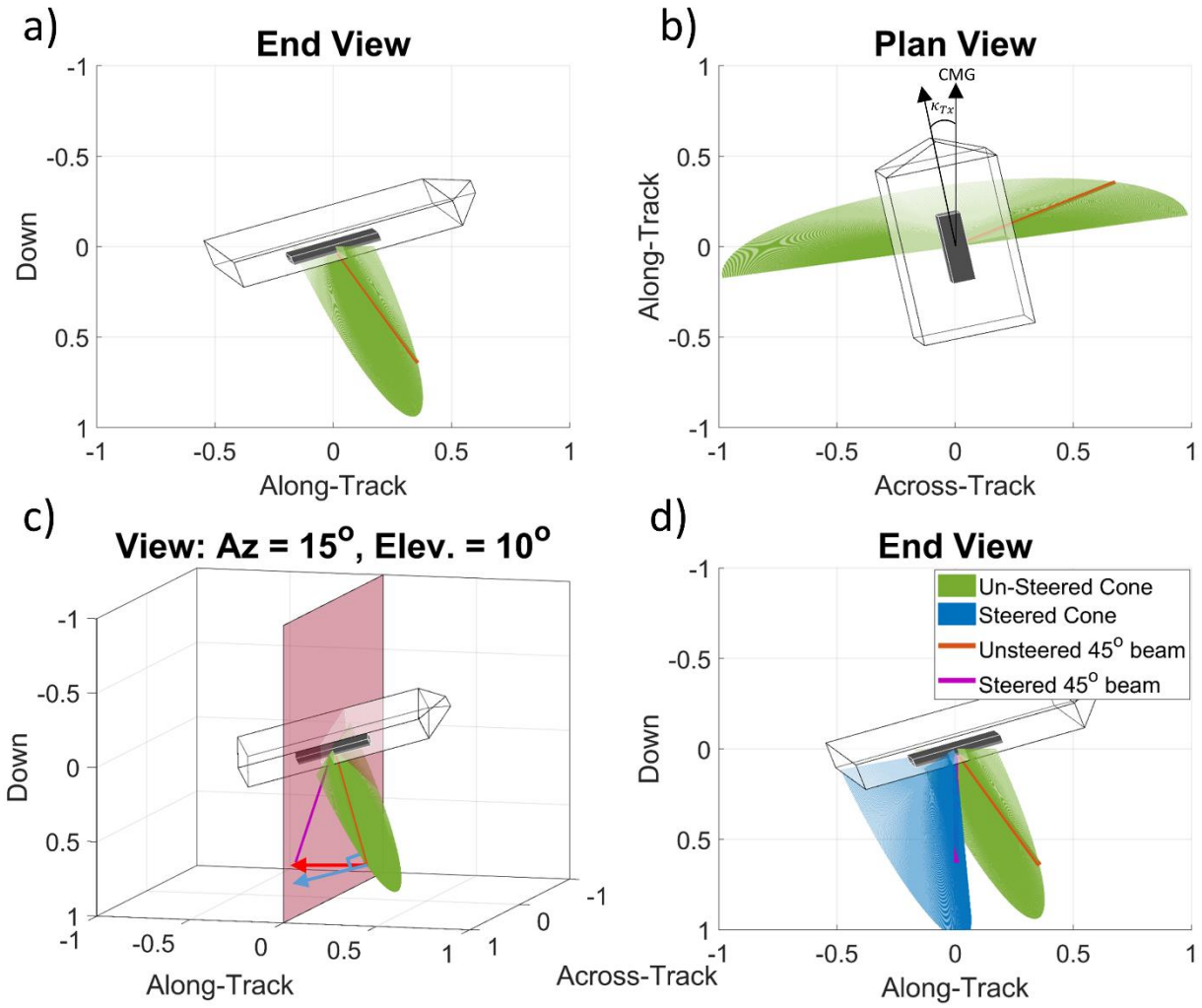

Figure 6: Along-track steering angle defined according to cone geometry. The along-track distance of an ideal across-track angle, θ_{Rx}^{MRF}, along the circumference of the un-steered cone (a, b) is used to calculated the along-axis steering angle required to bring the beam back to a desired along-track distance, here zero (c red plane). The resulting transmit steering angle simultaneously compensates for platform pitch and yaw, relative to the CMG (d). Each sector has a unique transmit cone.

The along-track angle is calculated using the un-steered beam's along-track displacement, (red vector, Fig. 6c), though strictly speaking, the distance along the transducer's axis should be used (blue vector, Fig. 6c). This discrepancy is minor for the small platform orientation angles expected, justifying the simplicity of the approach.

The underlying seafloor relief sinusoid is spatially parametrized in two-dimensions to allow for undulation along any heading, while angular and translational motions are temporally

parameterized. Horizontal vessel motion is not of interest to this study, and is therefore just modelled as a line to be consistent throughout the simulated "acquisition". The SSP is parametrized as a function of depth, having constant gradient, and is depth-interpolated for perfect surface sound speed (SSS) values at the multibeam array face. Finally, a geographic beam vector, $\mathbf{n}_{Geo}$, can be calculated for each sounding as originating from a multibeam reference frame defined as a concentric combination of the transmit and receive arrays' positions and orientations at their respective epochs [13]. TWTT is then determined numerically in simulation by tracking the resulting vector's refracted ray path until it intersects a model seafloor. This completely controlled environment provides a means of exactly quantifying the soundings' bathymetric errors.

2.1.1 – The Simulated True Seafloor

In order to determine a seafloor interaction fundamentally requires a remote surface. In the case of simulation, this may be replicated using a real world surface, such as a digital elevation model (DEM), or, more ideally for analysis, a mathematical surface, such as a parametric model. Simulation enables implementation of such a parametric model, which provides an exact bathymetric solution, and error, for an integrated sounding's horizontal location. Regional depths and curvatures are defined through two-dimensional sinusoids:

$$z = z_0 + a \sin(k\, x \sin\theta + k\, y \cos\theta)\,,$$

where:

- z_0 = mean depth,
- a = undulation amplitude,
- k = undulation wave number,

- x, y = horizontal coordinate in MRF,
- θ = undulation azimuth.

In this way, long wavelength curvature and short wavelength undulation in directions and with amplitudes of interest are created (Fig. 7). This facilitates evaluation of the robustness of RISC's combined error recovery model over various classes of bathymetry.

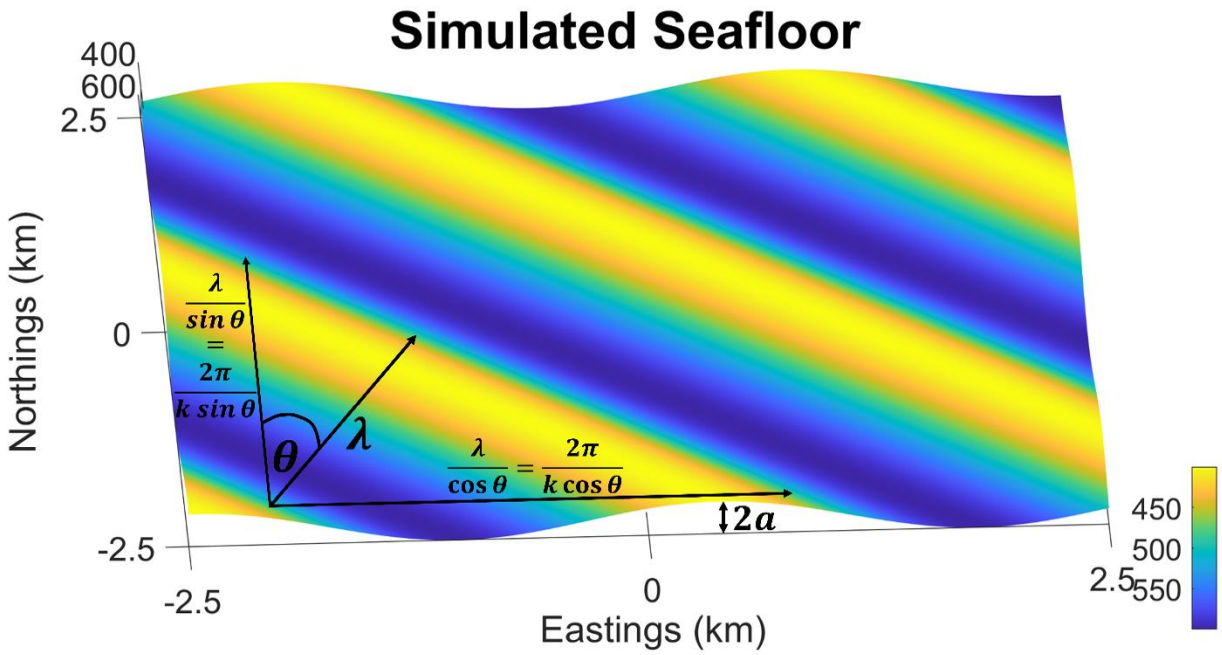

Figure 7: The designed synthetic seafloor, here treated as truth. This parametric model enables depth to be essentially "queried" at integrated sounding positions, both true and purposely erroneous, in order to exactly assess integration accuracy. Undulations at various wavelengths and desired maximum slopes defined according to the sinusoid's maximized spatial derivative are easily varied for analysis, as well as regional depth. View perspective: azimuth = -5°, elevation =30°.

This models depths as a nonlinear function of the mapping reference frame's (MRF's) horizontal coordinates, x and y. The impact of simulated seafloor undulation of various frequencies and maximum slopes on integration error estimates can be easily investigated in simulation by tweaking the sinusoid's parameters.

2.1.2 – An Inability to Perfectly Parameterize TWTT

The final requirement for integration is some time range that indicates how long the signal traces through the water column before interacting with the seafloor. Unlike all other inputs, this cannot be easily parametrized. A TWTT is measured in the field, and is necessarily a function of all input measures presented in Chapter 2.1, and the true inter-sensor offsets, analytical forms of which are presented in Chapter 3.1. Using a derived concentric geographic beam vector, the curvilinear ray path, and corresponding travel time, may be calculated through each horizontally stratified "layer" of the water column, as discretized by the sound speed profile (SSP) implemented in integration (Fig. 8). The curvilinear ray path through each layer is given by circular geometry, with refraction governed by Snell's law [14]:

$$C = \frac{\cos\varphi}{\mathrm{SSS}}$$

$$\mathbf{x}_{i+1} = \mathbf{x}_i + r_i \begin{bmatrix} (\sin\phi_{i+1} - \sin\phi_i)\cos\theta \\ (\sin\phi_{i+1} - \sin\phi_i)\sin\theta \\ -(\cos\phi_{i+1} - \cos\phi_i) \end{bmatrix},$$

$$r_i = -\frac{1}{C \cdot \Delta c_i},$$

$$\Delta c_i = \frac{(c_{i+1} - c_i)}{(z_{i+1} - z_i)},$$

having corresponding travel time [14]:

$$t_{i+1} = t_i + \frac{1}{\Delta c_i} \ln\left(\frac{c_{i+1}}{c_i} \cdot \frac{1 + \sin\phi_i}{1 + sin\phi_{i+1}}\right),$$

where:

- φ = initial depression angle, steered with the SSS measured at array face, c_0,
- $\phi_{i,i+1}$ = refraction angles entering and exiting the depth layer, as per Snell's law,

- $c_{i,i+1}$ = sound speeds bounding depth layer travelled through, via SSS sensor and SSP,
- t_{i+1} = sound's cumulative travel time through horizontally stratified layers.

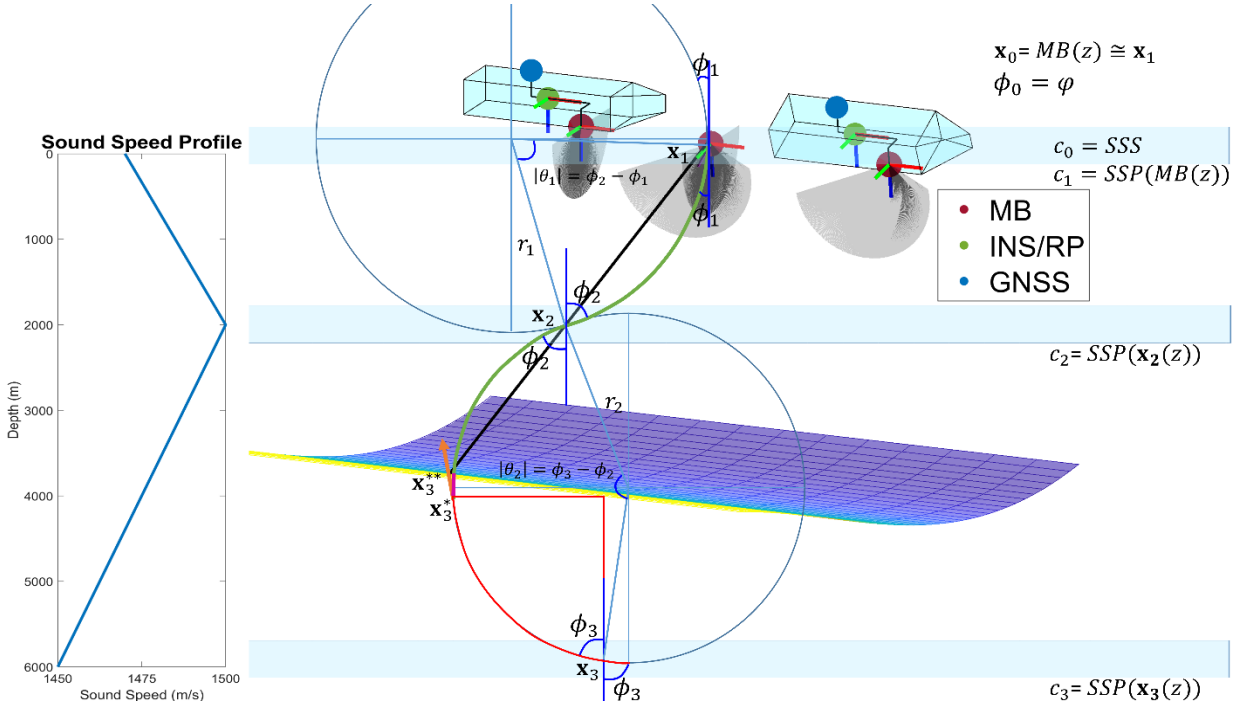

Figure 8: Ray trace procedure in the presence of seafloor relief. A cartoon ray trace illustrates a curvilinear path through a water column stratified into two layers. The green curve represents the true, curvilinear path, while the red and smaller magenta curves combine for the excess trace, culminating on the sound speed boundary at $\boldsymbol{x}_3$, which must be adjusted for. The orange vector is used to account for the final surface misclosure after adjusting the trace to $\boldsymbol{x}_3^*$ using the parametric depth queried at $\boldsymbol{x}_3$. This final adjustment provides the simulated sounding, $\boldsymbol{x}_3^{**}$. A hypothetical infinitesimal layer is added at the array face to implement a "snapback" of the depression angle from that calculated with the surface sound speed, φ, to that calculated with the sound speed profile measure at the array face, ϕ_1.

A special case is required for layers where $\Delta c = 0$, as well as those where the signal travels in a nadir direction, as both cause the radius of curvature to tend to infinity. This is trivially rectified by assuming the ray path to be a vertical vector, in which case the travel time through the layer is simply the average of its bounding sound speeds divided by the width of the layer.

In order to intersect the remote surface, thereby simulating a sounding, refractions are made at each depth-discretized sound speed until the seafloor is passed, at which point the surface is parametrically queried at the current sounding position (Fig. 8 $\mathbf{x}_3$). The result is used to adjust Δc, and ultimately the iteration of t_{i+1} and $\mathbf{x}_{i+1}$ in the ray trace, illustrated as $\mathbf{x}_{i+1}^*$ in Figure 8.

The effect of relief, however, is that the depth at $\mathbf{x}_{i+1}^{*}$ is likely to be different than that at $\mathbf{x}_{i+1}$, and an intersection is carried out to determine the final sounding coordinate on the parametric surface, (Figure 8 $\mathbf{x}^{**}{}_3$). The ray path is assumed linear over this small adjustment to the surface model. This depth is then used for an additional, final adjustment to Δc, preserving the depth-travel time relationship, though inducing a small horizontal error in soundings reintegrated with the resulting "true" travel time.

2.1.2.1 – Numerically Defined Soundings

Newton's method is selected to numerically estimate the depth of the final vector's and surface's intersection, as a function of horizontal position. Through equating the parametric surface and the depth component of the linearized final ray trace, $\mathbf{x}_{s+1} = \mathbf{x}_s + \Delta \cdot \mathbf{x}$ (Fig. 8 orange vector), and them both being in terms of horizontal position (x, y), the roots satisfying the equation indicate their three-dimensional intersection. The system is originally underdetermined as a result of there being only one equation of intersection and two variables. To circumvent this, the vector is projected into its x and y components, providing two orthogonal vectors which can then be simultaneously intersected with the parametric surface for their shared point of intersection. The two equations of the model, f_1 and f_2, are then given by:

$$\begin{bmatrix} f_1 \\ f_2 \end{bmatrix} = \begin{bmatrix} \mathbf{x}_s(z) + \Delta_{zx}\left(\mathbf{x_{s+1}}(x) - \mathbf{x_s}(x)\right) - \left(z_0 + a\sin(\kappa\, \mathbf{x_{s+1}}(x)\sin\theta_1 + \kappa\, \mathbf{x_{s+1}}(y)\cos\theta)\right) \\ \mathbf{x_s}(z) + \Delta_{zy}\left(\mathbf{x_{s+1}}(y) - \mathbf{x_s}(y)\right) - \left(z_0 + a\sin(\kappa\, \mathbf{x_{s+1}}(x)\sin\theta_1 + \kappa\, \mathbf{x_{s+1}}(y)\cos\theta)\right) \end{bmatrix}$$

$$= \mathbf{0}.$$

Quick visual inspection indicates no multicollinearity is expected unless the vector is traveling directly nadir, in which case the x and y component vectors become parallel. Thus, again a special case is required for nadir beams. A convenience of travelling in a nadir direction,

however, is there is no change in depth due to relief, and the initial ray trace convergence is perfectly accurate.

An iterative expression for the roots of a function is given by [18], which may be expressed in the following form:

$$\boldsymbol{f} = \boldsymbol{f} - \boldsymbol{J}_{\boldsymbol{f}}^{-\mathbf{1}}\boldsymbol{f},$$

where:

$$\boldsymbol{J}_{\boldsymbol{f}} = \begin{bmatrix} \frac{\delta f_1}{\delta x} & \frac{\delta f_1}{\delta y} \\ \frac{\delta f_2}{\delta x} & \frac{\delta f_2}{\delta y} \end{bmatrix},$$

is the first-order Jacobian, or gradient, of the two functions with respect to the independent variables. With the aforementioned special case for nadir, and only non-zero beam vectors expected, this matrix is generally invertible. Though the horizontal point of intersection attained by the vector is slightly imperfect relative to the curvilinear model's ray path, its impact is expected to be negligible for the small final adjustment typically expected for intersection. These roots are then used to evaluate the surface, simulating a sounding.

Integration of a remote sounding's position considers the orientation and position of the receiver at reception in order to estimate the geographic beam vector from the array-relative transmit and receive angles. This imposes a circular requirement since the reception time, and thus temporally-parametrized vessel state, cannot be determined for a particular sounding without first knowing the TWTT. Thus, a convergence scheme is designed with the receive vessel state initially defined identical to the transmit state. Updated receiver position and orientation, along with the sounding position and TWTT, are calculated until a satisfactory TWTT convergence of 1μs is reached. The corresponding TWTT calculated is reintegrated with integration errors

forced onto relevant inputs, creating datasets with known errors. These datasets are analyzed in Chapter 4.

A notable impact of this integration being dependent on the transmit and receive vessel states is that the resulting depth error is a combination of the integration error manifested at both epochs. This is addressed in section 2.2.1.

2.2 – Errors Remaining in Integration

High-frequency, motion-induced errors resulting from latency and scaling of INS output were first analyzed in the early nineties [19]. A deeper investigation into such motion dependent errors was undertaken by Hughes Clarke [2], where the impact of those integration errors, along with four additional common sources of significant, high-frequency depth errors were characterized:

1) GNSS-MBES X-lever error: $\Delta_{\mathrm{L}}(x)$,
2) GNSS-MBES Y-lever error: $\Delta_{\mathrm{L}}(y)$,
3) INS-MBES latency: Δ_t,
4) INS scaling: Δ_ρ,
5) INS-MB Z-axis misalignment: Δ_κ,
6) SSS Error (latency and/or bias): Δ_{SSS}.

Significant integration error is considered here to be that propagating with depth error greater than the particular sonar suite's bottom-tracking noise floor, currently at best around 0.1-0.2% of water depth [3]. This can vary widely according to depth-varying sonar configuration settings, including pulse length and type, as well as incidence angle, which all impact the bottom detection algorithm [3]. Commonly missed scales of the above spatial, temporal and angular

offsets can cause depth residuals on the order of 1-1.5% water depth [2], particularly when combined.

Each of the integration errors presented here acts to offset the estimated origin, and in some cases the orientation, of the multibeam, or more specifically its steered, virtual acoustic origin and beam vector. This is caused by erroneously transforming the auxiliary sensor data to the multibeam in integration. These errors were shown by Hughes Clarke [2] to each be primarily driven by unique components of platform motion (Fig. 9). As a result, theoretically they should be uniquely identifiable in soundings acquired by a vessel undergoing dynamic angular motion. Notably for error 5, the MB and the ship's VRF are assumed to be aligned, while the INS is unknowingly misaligned, resulting in incorrect lever arm values

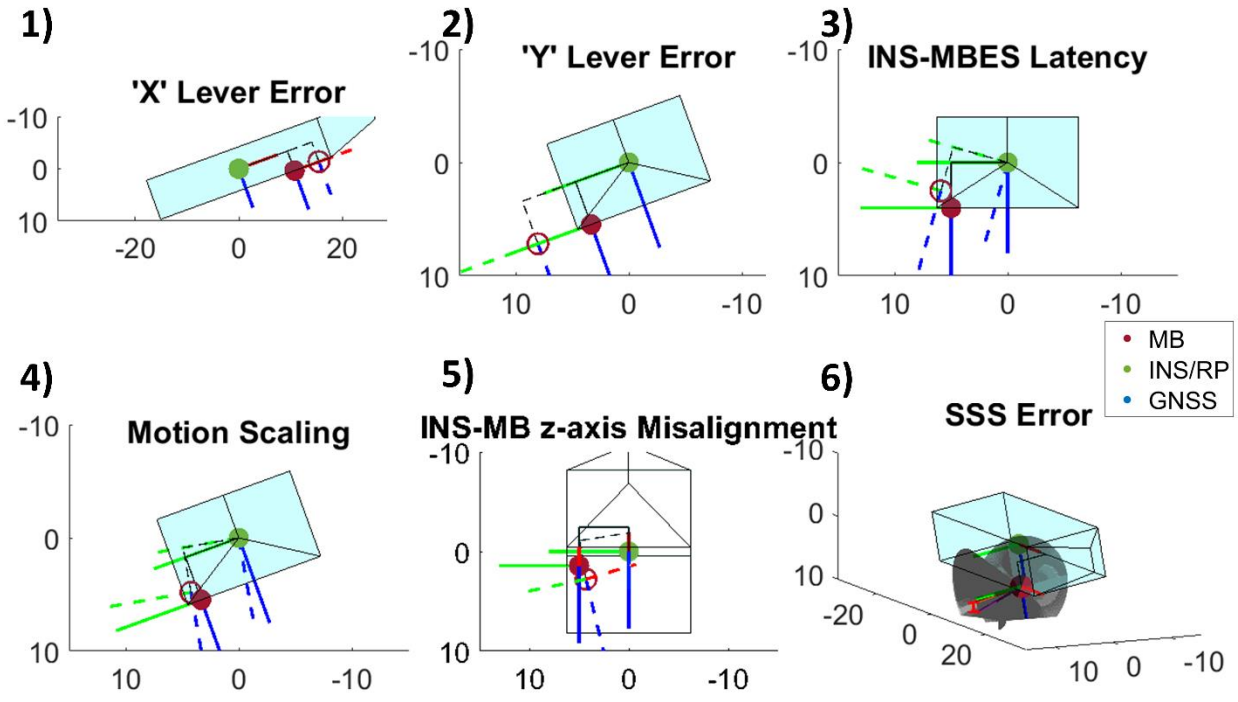

Figure 9: The impact of each of six integration errors presented in Hughes Clarke, (2003), at their symmetric error extrema when oscillating with a ten degree amplitude. Each subfigure number corresponds to each error in the above list.

Any resultant georeferenced sounding is derived from paired geometric components at transmit and receive time (Fig. 8). At those times, an INS/IMU provides orientation triplets and vertical

heave and a GNSS antenna provides horizontal position pairs, which are used to orient the array-relative steering angle relative to the multibeam's transmitter and receiver at their respective epochs.

The various errors in the modelled beam start point and vector then propagate to the integrated sounding as a three-dimensional position error (Fig. 10). Those integration errors propagating as an imperfectly orientated multibeam, namely errors 3 to 6 in the above list, scale with range and obliquity. In contrast, those causing only origin errors, errors 1 and 2, are not depth scaling and become increasingly insignificant with depth. As all the considered errors scale with the instantaneous orientation, the net result for periodic motion is a correspondingly periodic imprint of that error on the seafloor (Fig. 4) with a projected length scale which reflects the vessel displacement over the wave period. For example, a projected wavelength of 40 m would result from a 5 m/s vessel speed and 8 s wave period. In shallow water, where the shot-receive cycle is far shorter than the wave period, this projected wavelength undulates almost entirely along-track.

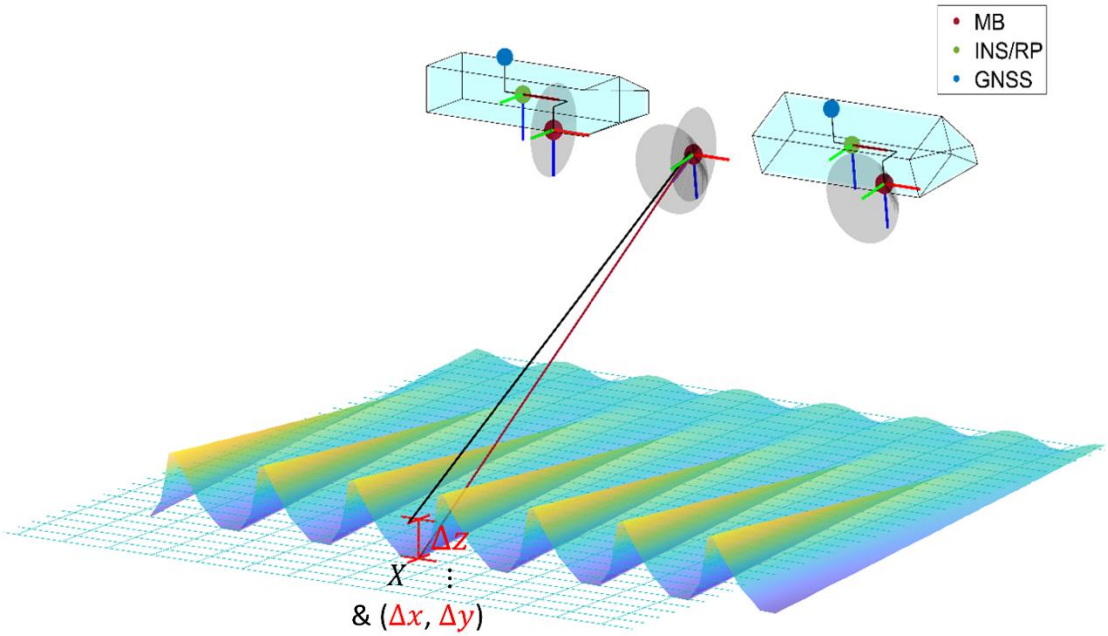

Figure 10: Illustration of geometric components required for integrating a sounding, and characteristic depth error resulting if an integration error exists. The multibeam's array-*relative angles, orientation triplets as observed by an INS/IMU, and three-dimensional positions observed by a GNSS antenna. These are each required at every sounding's transmission and reception, with two separate arrays observing the transmit and receive array-relative angles. Transmit and receive epoch separation, as well as the vertical axis scale are exaggerated for illustration.*

2.2.1 – Simulating "Wobbled" Swath Corridors with Numerically Defined TWTTs

"True" TWTTs are calculated using the previously described "inverse" ray trace. In order to simulated a swath corridor with the designed vessel motion and seafloor characteristics discussed in Chapter 2.1, multibeam configurations must be specified. Through defining a triple sector multibeam configuration, having 400 motion compensated beams, setting a ping rate according to 110% of the previous ping's maximum TWTT, and a 0.17ms delay between sectors, extensive swath corridors may be simulated. The first simulated ping is defined as occurring at $t = 0s$, while simultaneously defining the MRF's horizontal origin as that of the VRF's RP. Following this, TWTT is used to keep track of time, and the specified sensors, each rigidly aligned with the VRF, follow paths defined by the specified parametric models. Their orientations and positions are thus exactly defined for any given time.

This algorithm allows simple "acquisition" of ideal datasets, in particular their TWTTs, with which integration errors can be forced onto the "true soundings", provided they are appropriately designed into the georeference equation. These designs are presented in Chapter 3.1. Figure 11 provides an example of such a simulated dataset, where a 20ms INS-MB latency is forced onto the "true" integrations, or soundings. It is datasets such as this that are analyzed in Chapter 4.

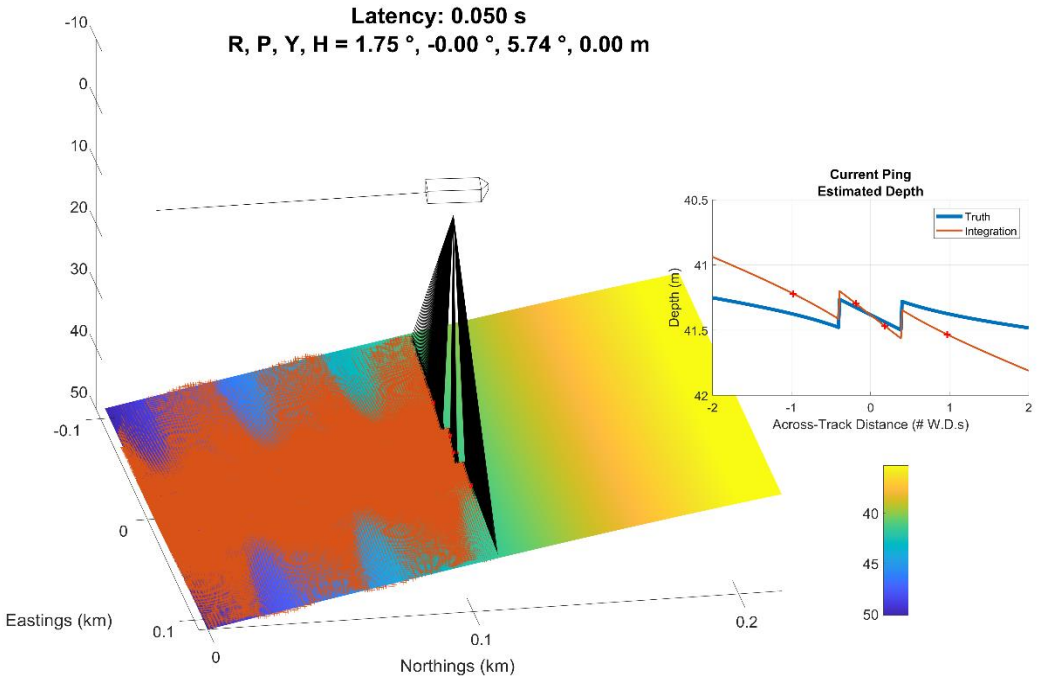

Figure 11: Erred output of multi-sector simulator developed to test the RISC approach. A 50ms motion latency has been applied, to "perfect" integrations, resulting in an error on the order of 1% water depth imposed on outer beams. This is on the order of the along-track discontinuities resulting from motion compensation in the presence of relief (inset). It is this erroneously integrated dataset which is used here for calibration.

Each integration errors' bathymetric signature can be exactly calculated in simulation by removing the parametric surface evaluated at the erroneously integrated sounding's horizontal location. These signatures are presented in Figures 12a and 12b when modelled over planes defined at 50 and 5000 m respectively. Propagated depth errors are illustrated for each error when sequentially driven uniquely by each relevant motion component: roll, pitch, yaw and heave. Implementation of a planar seafloor produces bathymetric errors which are identical to

sounding depth errors, which is subtly not the case in the presence of relief, as a result of their being a horizontal component to the propagated error.

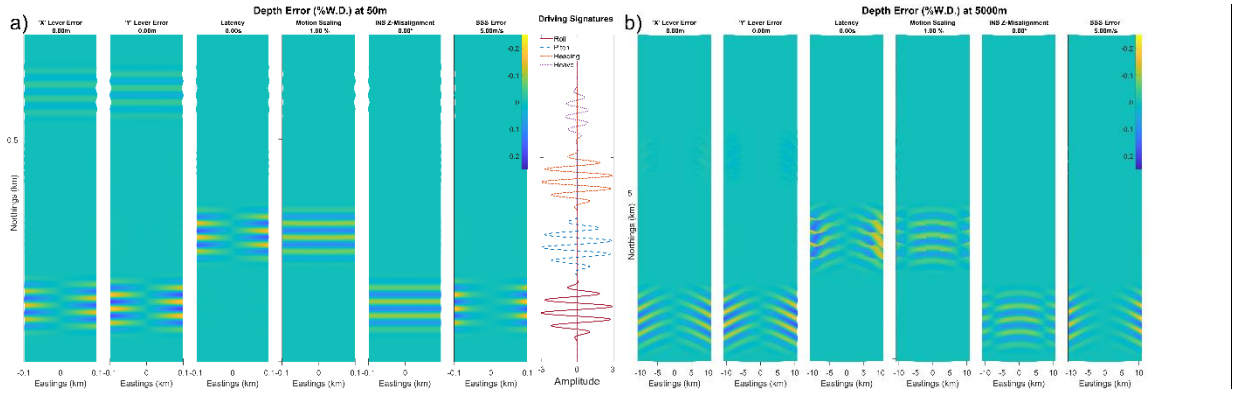

Figure 12: Bathymetric signature of each of the six integration errors when uniquely driven by eight second, three-degree sinusoids sequentially in roll, pitch and yaw and finally a one meter heave over a planar seafloor at depths of a) 50m; b) 5000m. Integration error magnitudes are such that they propagate as depth errors with peak amplitudes of approximately ¼ a percent of water depth (% W.D.). Along-track distance in b) is increased approximately an order of magnitude to illustrate deep water trends.

As depth increases, the change in the sonar's position and orientation over the shot-receive cycle increases. This is a result of pings having increasing travel time from source to seabed and back to receiver. This causes the character of the embedded integration errors to change, complicating the analysis of the depth residuals. In "shallow" water (50m in Fig. 12a), the manifest error is effectively constant for the entire ping, and thus the wobble appears orthogonal to the ship's track. In "deep" water (5000m in Fig. 12b), however, the error is clearly seen to evolve over the ping cycle, and thus is no longer exactly orthogonal to the ship track, instead migrating obliquely. As a result, the wobble has a projected undulation both along, and now, across-track.

It is clear that, as the water depth becomes greater the manifested depth error becomes increasingly nonlinear across-track, with the realized depth error evolving significantly as the vessel dynamically oscillates throughout the shot-receive cycle. This is the reason that the method of [2] was explicitly restricted to shallow water, where the ping period is short relative to the wave period. The method described herein, however, uniquely considers the relationship

between each sounding's error and the vessel state at both transmission and reception, thus removing this restriction.

2.3 – Review of Previous Work: Existing Swath Calibration Methods

In addition to characterizing the impact of each integration error, the first attempt to quantify these errors presented a computationally efficient calibration procedure, estimating the errors directly from a single swath corridor [2]. The assumption was that the corridor contained no real bathymetric roughness with dimensions close to the likely integration wobble. The approach opportunistically analyzed suitable swath corridor extents, by testing for and rejecting areas containing such "roughness", thereby producing increased redundancy in integration error estimates. This approach has the notable advantage of not requiring additional survey lines for calibration. The errors were estimated by assuming their signatures to be either across-track tilts or vertical departures of each ping from the running average, and linearly correlating that with each error's main driver existing at transmission, either: roll, roll rate, pitch or heave.

To be effective, the approach in [2] required:

A. the regional seafloor depth and slope be suitably removed from the analysis,
B. the sonar angular or depth anomaly being approximately constant for each beam across the swath,
C. only one of the more correlated error signatures existing (or at least dominating).

Requirement A is general for regression, where some suitable reference of truth is sought, against which residuals can be estimated and parameters adjusted. This was addressed in [2] by using across-track regressions of each ping, producing a series of depths and slopes, which were then high-passed filtered to remove the long wavelength seafloor signature, assumed to be real.

This assumed the seafloor to be planar across the ping, and the seafloor's sampled across-track slopes and depths to only be changing over time constants long with respect to the wave period. The locally planar condition is often reasonable for unconsolidated sedimented seafloors, but limits the class of seafloors suitable for calibration, particularly the peaks and troughs commonly expected in typical long wavelength bathymetry. Further, while the seafloor may be regionally planar, if tilted, with multisector systems, irregular distribution of each ping's soundings results from the combination of each sector's discrete acoustic pulse. This results in the across-track distribution of depths no longer fitting a plane (Fig. 5). The long time period assumption is not strictly true for a vessel yawing or pitching on an incline [2] (Fig. 9b and Fig. 9c respectively), and even more so with multi-sector stabilization. Figure 9c, the dataset which contains no integration errors, further illustrates average depth artefacts resulting from the rate of depth variation along-track being constantly changing over the high pass filter (HPF) window. Requirement B holds in shallow water conditions, such as 50 m, but, begins failing before 500 m as a result of the shot-receive cycle becoming significant relative to the driving wave period [2]. Finally, requirement C is an ideal situation, next to of course there being no errors at all. Failure of either of these significantly degrades results. The method developed here seeks to overcome these limitations, producing a calibration method more robust to the various classes of bathymetry acquired by ocean mappers.

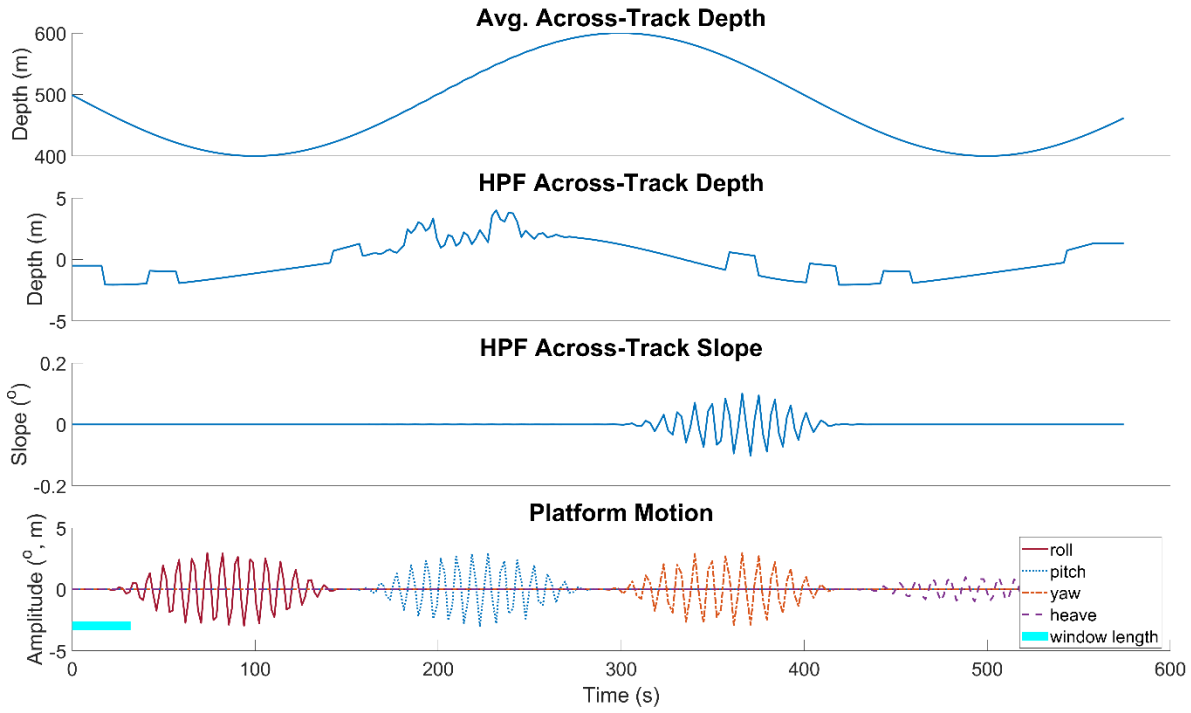

Figure 13: Artefacts in high-pass filtered time series of across-track depth and slope estimates observed when steaming over a long wavelength, purely along-track undulation. A low-frequency depth artefact results from using an along-track average to estimate the depth in the presence of the sinusoid's constantly varying curvature. A sporadic artefact occurs near the first derivative inflexion points, where the along-track average is a particularly poor sinusoid estimate. This misfit is exacerbated by spatially irregular sample of soundings. High-frequency depth artefacts result from using irregularly spaced pings to compute the moving window's average depth, obvious when pitching in the presence of along-track relief [1]. Slope artefacts resulting from yawing over a regional slope [1] are also clear.

Most literature on sonar integration calibration is geared towards identifying the sources of the, often more significant, static biases in observations. This has guided the development of field calibration routines which implement well-designed overlapping swath corridors to identify underlying errors ([20], [21], [22], [23], [24], [25], [26], [27], [28]). The general approach for adjustment is to minimize the deviation of soundings, either by examining point clouds ([20], [21], [22], [23], [25]), regressing onto planar patches ([24], [27]), and as well as onto a quadratic surface ([26], [28]).

Subsets of the integration errors investigated herein, particularly lever arms and INS latency, have been analyzed in sonar ([24], [26], [27], [28]), as well as lidar ([29], [30], [31], [32], [33]). With the exception of [28], in the case of sonar, only the patch test parameters of IMU-MBES

boresight misalignment and GNSS-MBES latency are considered. For that subset, even though the errors do have inter-dependencies, which might require simultaneous estimation to mitigate inter-error leakage, this is not necessarily required for the patch test. Through the use of carefully paired line geometries and specific stepwise estimation and application of the calibration parameters, errors other than that of current interest cancel out ([20], [21]). In contrast to the simpler patch test approaches, the referenced lidar methods, and more recent sonar approaches ([24], [26], [27], [28]), implement a mathematical model coupling the error terms. A gradient method, such as iterative least squares, is then applied for nonlinear optimization relative to some ground truth. The sonar approaches, apart from [28], all implement overlapping swaths to define said reference, however, which the method described here seeks to avoid for mission efficiency, while increasing the availability of suitable data.

The lidar community demonstrated that the extensive smooth surfaces often found in nature can be effectively modelled by fitting low order polynomials over extended spatial extents of scattered measurements [30]. Such surfaces are thus often suitable for calibration of systems acquiring scattered measurements. The approach, however, implemented *a priori* definition of surfaces using higher accuracy RTK GNSS observations, a luxury which pioneering ocean mapping missions do not have. Extension to sonar systems has seen the use of in situ data to simultaneously estimate such surface models ([26], [27], [28]).

The most recent multibeam calibration procedure [28] implements an approach which, similarly to that in [2], estimates the integration error using only a single swath corridors' soundings. Whereas [2] implements two-dimensional seafloor detrending by high pass filtering a series of across-track fitted lines, [28] fits a quadratic surface along the swath corridor. A mathematical integration model is necessarily employed to account for the evolution of the propagated error

signature over the extended along-track domain. This uniquely analyzes each sounding's input-error relationship within the domain similarly to early lidar calibration techniques which first calibrated against such surface features with scattered measurements. An iterative least squares adjustment is then implemented to optimize the sounding depth misclosures as a function of latency. Notably, however, this is the only parameter solved by the method. In contrast, the approach presented here addresses six parameters simultaneously.

III – RIGOROUS INTER-SENSOR CALIBRATOR (RISC)

Considering the high spatial frequency of the propagated motion-dependent integration errors overprinted the seafloor, [2] and [28] proposed that a single swath corridor is sufficient for analysis, once underlying assumptions of suitable seafloor and vessel motion are achieved. Wave-driven, high-frequency vessel motion and low frequency seafloor undulation combine to produce conditions in which each error's propagated "wobbles" quickly decouple from each other, as well as the seafloor. A requirement for calibration through optimization, as is presented here, is to have a suitable reference of the true seafloor. The algorithm presented here is designed to simultaneously identify the six integration errors, while accurately modelling the seafloor.

3.1 – Coupling of Errors with a Georeference Model

Though [2] demonstrated the correlated errors can often be identified and solved in a stepwise manner, starting with the most significant, this approach seeks to simultaneously estimate each. The across-track depth error becomes a nonlinear function of each of the integration errors when more than one error is present and thus a coupled model is required to distinguish them.

The coupling of integration errors for calibration of swath systems was undertaken by the lidar community ([29], [30], [31], [32], [33]) who then implemented various stochastic models to minimize the spread of those observations relative to surface features, typically planes. A georeference model including the errors provides a means of analyzing the relationship between the input to each point measurement and the resultant manifest error. By utilizing multiple points, typically several thousand, over an extended domain such as a swath corridor, this relationship typically increases the over-determination of calibration parameters. Such an approach is equally suited to both shallow and deep water conditions, where the realized depth

error begins to evolve across individual pings. Furthermore, this approach is able to better manage the dependent nature of the errors, as they are simultaneously estimated using the coupled model. The stochastic model can be extended to consider the correlations among the integration errors within the local sample [33], and is recommended for field implementation. Published sonar calibration techniques ([24], [26], [27]) have similarly implemented a coupled georeference model. The sounding may be represented simply by an origin and vector, defined in polar coordinates:

$$\mathbf{x} = \mathbf{MB}^{\mathrm{MRF}} + s \begin{bmatrix} \cos(\phi + \phi_R)\cos\theta \\ \cos(\phi + \phi_R)\sin\theta \\ \sin(\phi + \phi_R) \end{bmatrix}$$

where:

- $\mathbf{x} =$ Sounding coordinate,
- $\mathbf{MB}^{\mathrm{MRF}} =$ Position of multibeam's virtual acoustic center in mapping reference frame,
- $s =$ Slant range to sounding,
- $\phi =$ Initial depression angle of transmission,
- $\phi_R =$ Additional depression angle to sounding due to water column refraction,
- $\theta =$ Azimuth of transmitted echo, or acoustic return.

Every sonar integration package has to have some form of the above georeferencing implementation, although it is not typically accessible from proprietary packages. To be specifically useful for least squares optimization, however, the implementation has to allow for the partial derivatives of the integrated sounding relative to each integration error to be accessible. This requires an analytical representation of the georeference model's solution, including its ray trace component, which that presented above achieves using variables s and ϕ_R.

The above representation also helps easily distinguish the integrated beam vector and ray trace components of the solution, useful in calculation of the derivatives. Though not done here, simply adjusting the direction vector and ignoring the adjustment to the ray trace range, s, and departure, ϕ_R, provides a far quicker, though slightly less accurate adjustment procedure.

This thesis uses the swath corridor simulator discussed in Chapter 2.1 to produce ideal datasets for analysis. This simulator implements a concentric intersection of the transmitter and receiver's cones of sensitivity which accounts for the non-orthogonality between them, such as that seen in [13]. The sensor inputs previously described, and how they contribute to the final sounding position, **x**, is illustrated in Figure 14. This generic georeference model implies the signal follows the same path to and from the seafloor, requiring only one sequence of refractions for integration.

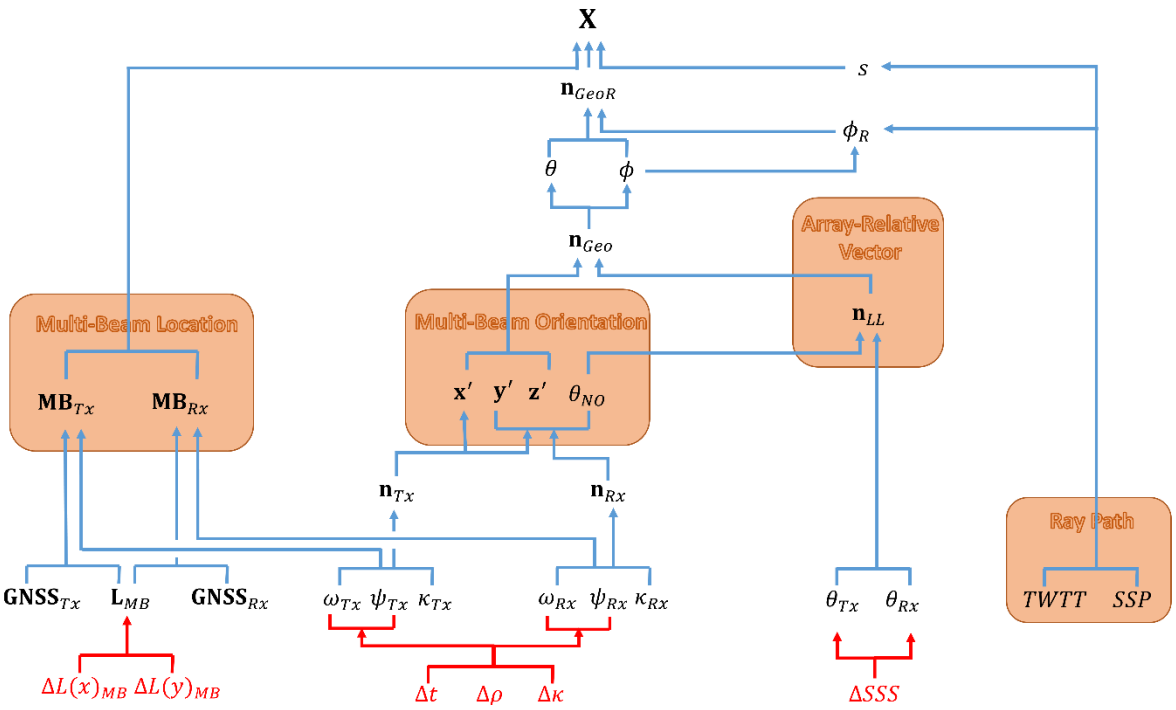

*Figure 14: Flowchart of a non-orthogonal, concentric intersection of the transmitter (n_{Tx}) and receiver (n_{Rx}) arrays' cones of sensitivity. The cones are steered to angles θ_{Tx} and θ_{Rx} respectively to georeference a remote seafloor interaction, **X**. Two variables, ϕ_R and s are employed to account for water column refraction and equating time ranges to distance respectively. The additional terms in red at the bottom are the six errors fed into the model.*

This simplified concentric model is sufficient for analyzing the characteristics of the integration error signatures, particularly in the simulated environment presented here, where the true sounding positions are actively defined by the model. Simulation provides a closed environment, ideal for analyzing the "wobble" imposed on bathymetry acquired under various input combinations. Here, simple parametric models are implemented which are meant to represent environmental conditions. Results can then be used to assess the proposed method's theoretical capability to simultaneously determine the sources of wobble in various classes of environment, with capability in various water depths, seafloor undulation wavelengths, and angular vessel motion magnitudes and rates being of particular interest. Such assessment is possible through comparison of error estimates to their known, forced values. Implementation on field should use a non-concentric model, which is more representative of reality.

The integration errors' impact on bathymetry can be characterized by their effect on the position and orientation observations when transformed from the auxiliary GNSS antenna and INS/IMU respectively, to the multibeam's reference frame. This concentric combination of the transmit and receive arrays at their respective epochs creates a single reference frame representing a virtual multibeam from which the signal is transmitted and received [13]. The parametrically-linear impact of each error was already presented in [2]. Those same errors are here included in the georeference model through adding them into the auxiliary sensor inputs:

$$\omega_i^* = \sin^{-1}\left(\cos \Delta_\kappa \sin\left(\Delta_\rho\left(\omega_i - \frac{\Delta\omega_i}{\Delta t_i}\Delta_t\right)\right) + \sin \Delta_\kappa \sin\left(\Delta_\rho\left(\psi_i - \frac{\Delta\omega_i}{\Delta t_i}\Delta_t\right)\right)\right),$$

$$\psi_i^* = \sin^{-1}\left(\cos \Delta_\kappa \sin\left(\Delta_\rho\left(\psi_i - \frac{\Delta\psi_i}{\Delta t_i}\Delta_t\right)\right) - \sin \Delta_\kappa \sin\left(\Delta_\rho\left(\omega_i - \frac{\Delta\psi_i}{\Delta t_i}\Delta_t\right)\right)\right),$$

$$\kappa_i^* = \kappa_i - \frac{\Delta\kappa_i}{\Delta t_i}\Delta_t,$$

$$Hv_i^* = \Delta_\rho\left(Hv_i - \frac{\Delta Hv_i}{\Delta t_i}\Delta_t\right),$$

where:

- $(\omega_i^*, \psi_i^*, \kappa_i^*)$ = Adjusted orientation triplet measured by auxiliary INS/IMU sensors,
- Hv_i^* = Adjusted heave output by INS, assigned to $\mathbf{GNSS}^{MRF}(z)$
- $\left[\frac{\Delta\omega_i}{\Delta t_i}, \frac{\Delta\psi_i}{\Delta t_i}, \frac{\Delta\kappa_i}{\Delta t_i}, \frac{\Delta Hv_i}{\Delta t_i}\right]$ = roll, pitch, heading and heave rates via raw high frequency input.

These measures are then transformed to the multibeam arrays for integration. For the sake of simplicity, assuming the transmitter, $\mathbf{n}_{Tx}$, and receiver, $\mathbf{n}_{Rx}$, to be respectively parallel and perpendicular to the vessel reference frame (VRF) eliminates the need for including their alignment relative to the INS and gyro for integration, though this could be easily added.

These modified output angles are also applied in both orienting the multibeam relative to the position source, typically either the GNSS antenna or vessel reference point (RP). This gives the position of the virtual, concentric multibeam array, as an average of the transmitter and receiver positions at their respective epochs:

$$\mathbf{MB}_i^{MRF*} = \frac{1}{2}\left(\mathbf{GNSS}_{i,\,\boldsymbol{Tx}}^{MRF} + \mathbb{R}(\kappa_i^*, \psi_i^*, \omega_i^*)_{Tx}(-\mathbf{GNSS}^{VRF} + \mathbf{Tx}^{VRF} - \boldsymbol{\Delta}_L)\right)$$

$$+\frac{1}{2}\left(\mathbf{GNSS}_{i,\,\boldsymbol{Rx}}^{MRF} + \mathbb{R}(\kappa_i^*, \psi_i^*, \omega_i^*)_{Rx}(-\mathbf{GNSS}^{VRF} + \mathbf{Rx}^{VRF} - \boldsymbol{\Delta}_L)\right),$$

where:

- $\mathbf{GNSS}_{i,\,Tx/Rx}^{MRF}$ = position in mapping reference frame (MRF) at transmission/reception,
- $\mathbb{R}(\kappa_i^*, \psi_i^*, \omega_i^*)_{Tx/Rx}$ = rotation from transmitter's/receiver's reference frame to MRF using adjusted orientation triplet (heading, pitch, roll),
- $-\mathbf{GNSS}^{VRF} + \mathbf{Tx}^{VRF}/\mathbf{Rx}^{VRF}$ = GNSS-MB transmitter/receiver lever arms in VRF.

Finally, the actual steered array-relative angles, that are combined to geographically orient the transmitted signal, are themselves impacted by surface sound speed estimates:

$$\theta_{Tx}^* \approx \sin^{-1}\left(\frac{SSS - \Delta_{SSS}}{SSS}\sin\theta_{Tx}\right),$$

$$\theta_{Rx}^* = \sin^{-1}\left(\frac{SSS - \Delta_{SSS}}{SSS}\sin\theta_{Rx}\right).$$

A consequence, however, of using a flat array in a horizontally stratified fluid is that the errors in the estimated array-relative steering angles are almost entirely corrected when the sound speed used in refraction converges to the truth, typically at depth ([2], [34]). This uses the a SSS measured at the array face to accurately calculate the transmission's Snell's constant that is implemented in the ray trace [35], and conveniently assuming a perfect sound speed profile, this correction adjusts the error in the steered portion of the geographic depression angle after the

snapback layer refraction. The result is a motion correlated error which is eliminated whenever the array is level. The purely SSS error is propagated as:

$$\theta_{Tx}^{*} \approx \sin^{-1}\left(\sin\left(\theta_{Tx} - \psi_{Tx}\left(1 - \sqrt{\sin^2\theta_{Rx}}\right)\right) + \frac{SSS - \Delta_{SSS}}{SSS}\sin\psi_{Tx}\left(1 - \sqrt{\sin^2\theta_{Rx}}\right)\right),$$

$$\theta_{Rx}^{*} = \sin^{-1}\left(\sin(\theta_{Rx} - \omega_{Rx}) + \frac{SSS - \Delta_{SSS}}{SSS}\sin\omega_{Rx}\right).$$

These terms can be integrated into any georeference equation and the soundings' sensitivities with respect to the parameters can be analyzed for optimization. Notably the along-track error component, which is typically far smaller than the across-track component, is a simplification of the motion compensation equation presented in Chapter 2.1, assuming zero yaw.

3.2 – Suitable Truth; Flattening Residuals to Local Natural Surfaces

In order to have a good estimate of each instantaneous beam depth error, a model of the true seafloor is required as a reference. In the absence of an independent truth, such as an overlapping perfect survey, this approach attempts to extract the true seafloor from the imperfect observations themselves, producing a rigorous calibration scheme. The key is to have a seafloor model that is immune to the sought imperfections in the observations, and of course a seafloor which the model suitably approximates. As discussed, any integration error will be projected with a characteristic spatial length scale, directed primarily along-track, and thus seafloors that contains only depth variations over significantly longer wavelengths are sought.

3.2.1 – The Seafloor as a Quadratic

While the seafloor may be reasonably filtered through along-track high pass filtering of a series of across-track linear regressions [2], it has been demonstrated that, provided smooth, regular bathymetry a quadratic surface effectively estimates the underlying natural seafloor surface using

a swath corridor containing high frequency bathymetric errors [28]. A surface-based approach simultaneously filters along-track and across-track seafloor trends and is expected to better account for the irregular along-track distribution of soundings than [2] while being characteristically different from the oscillatory wobble signatures. Using a surface as opposed to a line feature further allows for integration error estimates to be made using extents of swath corridor as opposed to a single ping, thereby increasing domain size. This generally produces more stable solutions. Considering such extended domains requires an error recovery model which analyzes the relationship between each sounding's input and error, as the manifest integration error is no longer constant within the domain.

This thesis proposes a combination of a quadratic model as the estimate of the true surface, together with the presented coupled georeference model, so that error estimation can proceed. This produces an equation for regression which can account for the variation in the error's driving signature within the regression domain, predominantly vessel orientation. Considering a standard stochastic model:

$$\epsilon = y - h(\mathbf{x}, \boldsymbol{\beta}).$$

Expanding the model and its disturbance terms to consider both the sounding and seafloor components, and constraining the difference to be zero at every sounding provides the expression to be minimized,:

$$\left(\epsilon_s - \epsilon_q\right) = 0 - \left(f(\mathbf{x}_{\boldsymbol{s}}, \boldsymbol{\beta}_{\boldsymbol{s}}) - g\left(\mathbf{x}_{\boldsymbol{q}}, \boldsymbol{\beta}_{\boldsymbol{q}}\right)\right) = \Delta z(\mathbf{x}, \boldsymbol{\beta}),$$

where:

- $f(\mathbf{x}_{\boldsymbol{s}}, \boldsymbol{\beta}_{\boldsymbol{s}}) = \mathbf{MB}^{\mathrm{MRF}*}(z) + s\sin(\phi + \phi_R)$,
- $g\left(\mathbf{x}_{\boldsymbol{q}}, \boldsymbol{\beta}_{\boldsymbol{q}}\right) = \beta_0 + \beta_1 x + \beta_2 y + \beta_3 xy + \beta_4 x^2 + \beta_5 y^2$.

Minimization then in effect seeks to "flatten" the soundings to the quadratic surface. Considering each sounding's residual (Fig. 10) has the added benefit of eliminating the need to limit analysis to shallow water conditions, since the temporal evolution of the propagated "wobble" among the soundings is now accounted for.

3.2.1.1 – Gauss-Newton Optimization:

For this preliminary study of the method's validity, a simple Gauss-Newton approach is taken to optimize the sum of squares: $\boldsymbol{\epsilon}^T\boldsymbol{\epsilon} = h(\boldsymbol{X},\boldsymbol{\beta})^T h(\boldsymbol{X},\boldsymbol{\beta})$. This cost function is then linearized through first order Taylor expansion about $\boldsymbol{\beta_0}$, the current estimate of the integration errors, providing, through linear algebra, an iterative solution for $\boldsymbol{\beta_1}$ an, ideally improved, least squares estimate of the true integration errors, $\boldsymbol{\beta}$:

$$\boldsymbol{\beta_1} = \boldsymbol{\beta_0} - (\boldsymbol{X'^0 X^0})^{-1}\boldsymbol{X^{0'}}\, h(\boldsymbol{X},\boldsymbol{\beta_0}),$$

where $\boldsymbol{X^0} = \boldsymbol{\delta} h(\boldsymbol{X},\boldsymbol{\beta_0})/\boldsymbol{\delta\beta_0}$. Notably, this least squares model implies that the depth errors are entirely determined by the Taylor series linearization, the sampled input, $\boldsymbol{X}$, and the current estimates of the parameters considered in the model, $\boldsymbol{\beta_0}$, here the integration errors as well as the quadratic surface trends. Parameter and input uncertainties are disregarded here, as optimization efficiency is not the goal of this Master's thesis. Rather, the goal is to seek conditions under which asymptotic convergence to an *a priori* known truth occurs.

Each observation equation, the residual between the modelled sounding and quadratic surface, provides additional information for determining the relationship between observed bathymetric errors and their driving signals as per the model design. Soundings attained from various states of vessel orientation and depth in the water column are required to increase the amount of independent information within the optimization scheme. As depth increases, the variation in vessel state for a given number of contiguous soundings, and thus the independence of

observations, increases, thereby reducing the number of observations required for successful estimation and satisfactory confidence in results. The total number of observations acquired, and thus total information available, however, decreases with depth.

3.2.1.2 – Suitability of Smooth Seafloors:

The desire for long wavelength undulation is twofold. First, it is characteristically different from short wavelength wobble, and second, it is expected to have slowly varying slope and curvature, the very parameters the quadratic surface seeks to estimate. Considering the quadratic surface as a polynomial filter, and sinusoidal seafloor undulation, the shortest wavelength seafloor capable of being satisfactorily filtered in analysis is twice as long as the window length, both across-track and along-track. This is in accordance with Nyquist folding frequency, which sees low-order polynomials removing half the spectral power (3dB) of any undulation with wavelength twice as long as the local moving window [36], removing increasingly more power for longer wavelengths. The two dimensional quadratic here acts as such a window. With the expected subtlety of the integration errors, this two window length minimum for undulation wavelength is unlikely to suffice in the presence of seafloors trends which correlate with the errors. The subtlety of the depth errors typically calls for high accuracy seafloor models, as the errors can be easily obscured by remnant seafloor undulation and roughness. Long-wavelength undulations, preferably many times more than twice the window length, are thereby recommended, such that they are increasingly. By the same reasoning, a window length larger than twice the wobble wavelength is also desirable, ensuring more of the subtle wobble signature is precluded from filtering.

Figure 15 presents a quadratic surface fit to a sinusoid, gently rolling along-track with a 2 km wavelength and 25 m amplitude. The proposal is that a window length of 1 km should remove

half the power, or intensity, of that undulation, with the other half leaking into the analyzed depth residuals. For the subtle errors being analyzed, however, a far shorter window is desired to better fit, and thus further filter the seafloor undulation. Here, a window length of three wave periods, or 120 m when steaming at 5 m/s is implemented, and found to suitably adhere to the underlying sinusoid. This is assessed through convergence of the depth residuals relative to the quadratic surface, to the true depth errors relative to the underlying sinusoid. Their convergence is illustrated top right. Notably, too short of a window will begin to follow the wobble itself, producing inaccurate estimates of the true depth misclosures.

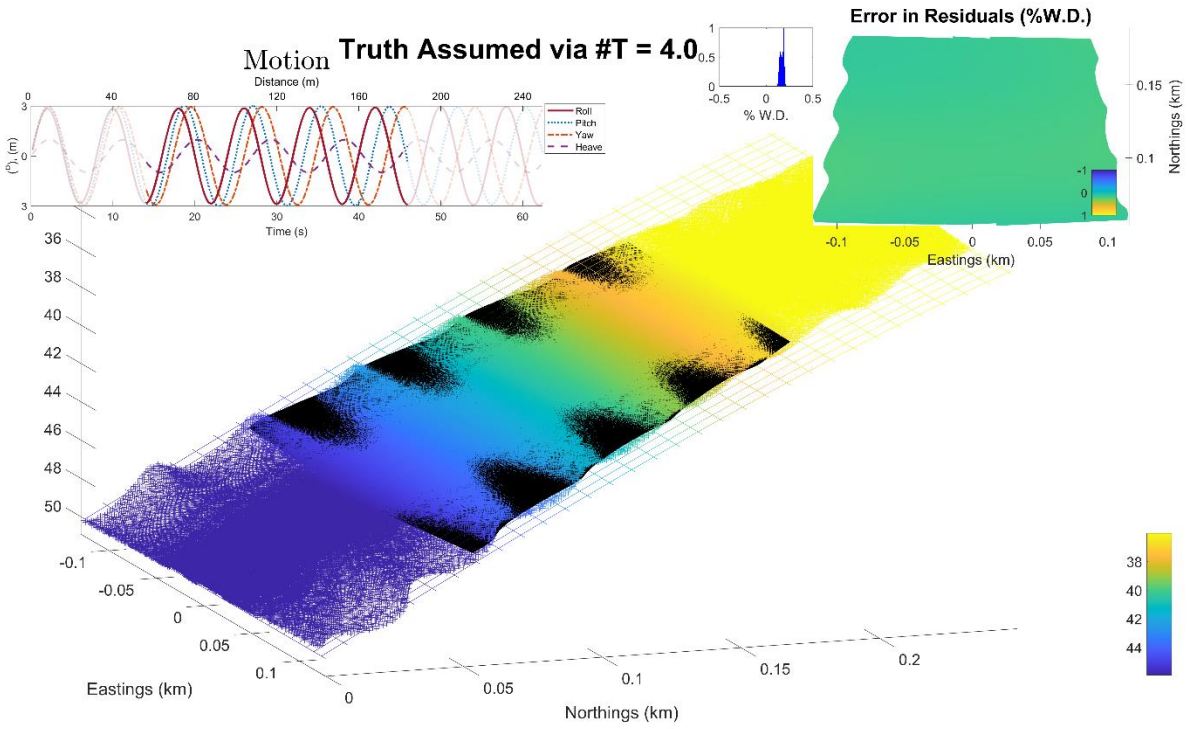

Figure 15: Swath corridor simulated with six simultaneous errors and driven by the motion time series illustrated top left. A subsection of wobbled swath corridor, spanning three wave periods, or 120 m (relief-colored crosses) is used to approximate the true underlying seafloor (relief- colored mesh). Top right illustrates the ratio of depth misclosures estimated relative to the quadratic surface versus the sinusoid, taken as truth. A zero magnitude surface illustrates a perfect quadratic fit.

It is important to realize here that a quadratic surface, with only one inflexion and associated curvature across-track, and another along-track, can never perfectly fit a sinusoid, as there are

multiple inflexions and the curvature constantly changes. Thus, from a quadratic fit point of view, the domain would ideally be no more than about ¼ of the sinusoid wavelength. While the quadratic may not perfectly fit the seafloor, a notable implicit advantage is that it is restricted to one inflexion along-track and another across-track, thereby quickly decoupling from the oscillatory motion-dependent errors projected onto the seafloor. This ensures the surface does not overfit the observations, potentially absorbing the wobbles.

3.2.2 – A Need for Local Analysis

While domains spanning significant time are desired to distinguish the ambiguous integration errors, domains spanning short spatial extents are desired to more strongly filter the seafloor. A balance must be found.

By considering extended domains, and thereby many thousands of point observations, typically the level of over-determination grows, and thus confidence in the calibration parameters estimates. Figure 16 illustrates estimate accuracies for a domain spanning three wave periods, here 24 seconds, versus six wave periods, or 48 seconds. Here all errors are simultaneously forced while the vessel heaves and oscillates in each component direction. Results reassuringly illustrate that solutions converge as more information is added to the system. Local confidence intervals are extremely small due to the large number of soundings. The dependence of the soundings imply that that these intervals are underestimated.

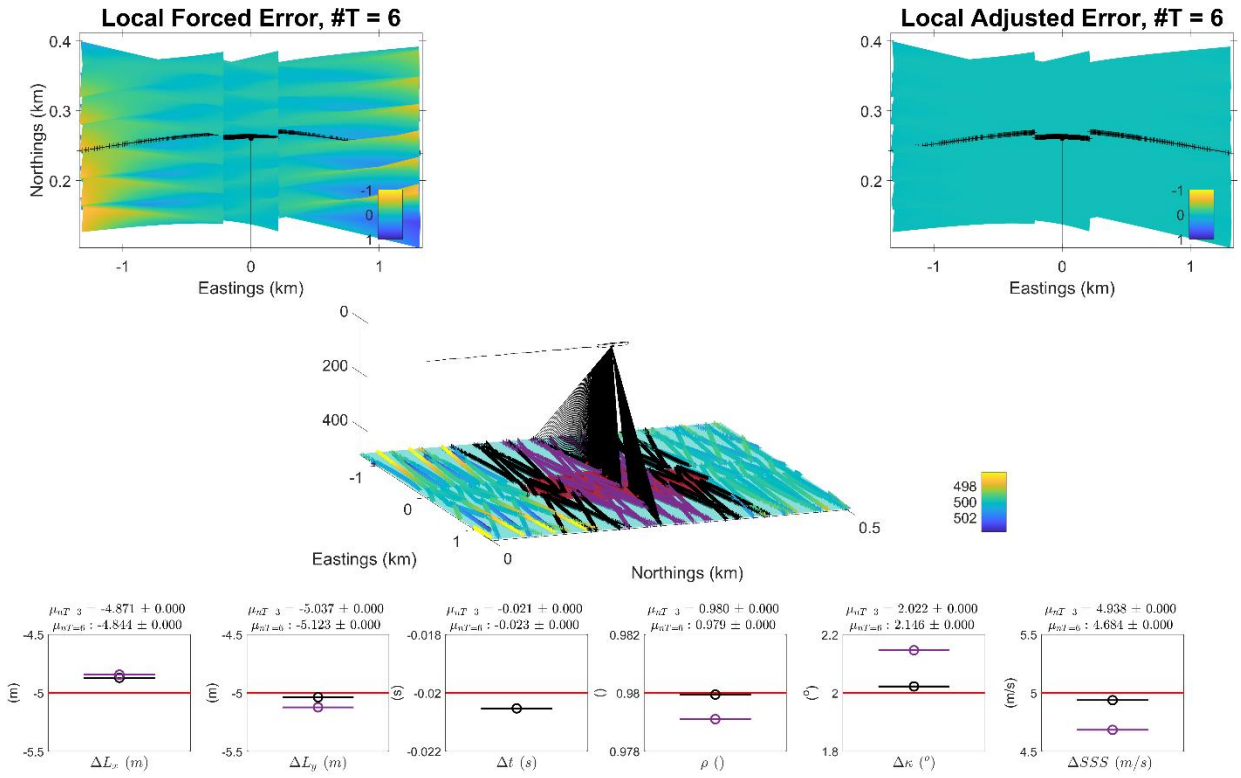

Figure 16: Here the rigorous inter-sensor calibrator (RISC) is applied to the wobbled soundings simulated over a planar seafloor at 500m depth. The vessel is oscillating in all three angular components as sinusoids with three-degree amplitude and eight second period. All six errors are present with magnitudes indicated by the red line. The 24 and 48 second estimates are in purple and black respectively, as well as their associated soundings. Boxplot axes are $\pm$10% error magnitude in each case.

Typical seafloors, however, are not always planar. While a seafloor containing only long wavelength undulation is desired, seabed geology changes spatially, and the regional seafloor

may contain a wide spectrum of undulations. This includes slowly evolving wavelengths, as well as regions where distinct features may suddenly arise in otherwise gently rolling seafloor, such as bedrock outcrops and sand waves. The first case of a slowly evolving undulation wavelength should not pose an additional problem, since the algorithm is already considering a suitably long wavelength undulation, ensuring the seafloor slope and curvature do not significantly change over the regressed section of swath corridor. Fast changes in seafloor complexity, however, induced by the sudden appearance of high frequency features, are likely unsuitable for analysis. This is because a simple quadratic model cannot account for variation in the trends it seeks to estimate.

Notably, remnant seafloor undulation not accounted for by the quadratic fit, particularly natural roughness occurring at the scale of the projected wobble, can artificially correlate with the propagated integration errors. Further, a consequence of using an approach which estimates the true seafloor with only non-overlapping swath corridors acquired in situ, is that errors propagating as low frequency, or static, depth errors are absorbed by the quadratic fit, and cannot be analyzed without suitable overlap of the swath corridor. This specifically applies to the multibeam misalignment parameters determined by the patch test.

Figure 17 illustrates a typical region of continental shelf bathymetry that exhibits seafloor undulations over a wide range of natural spatial wavelengths, some suitable, some not for this analysis. One can see both real natural roughness (Fig. 17 short λ A) as well as periodic integration artifacts (Fig. 17 short λ B) at similar length scales. There exist extensive regions, however, that do not contain that natural roughness. Examples shown are areas that are near flat (Fig. 17 planar), and those with medium or long wavelengths, relative to that of the wobble. These all arise within a three-kilometer square region of seafloor. Thus, instead of optimizing an

entire swath corridor, local regression of short sections is proposed. The simulated bathymetry used in this paper, reproduces sinusoidal morphology at these typical, longer length scales (>300m).

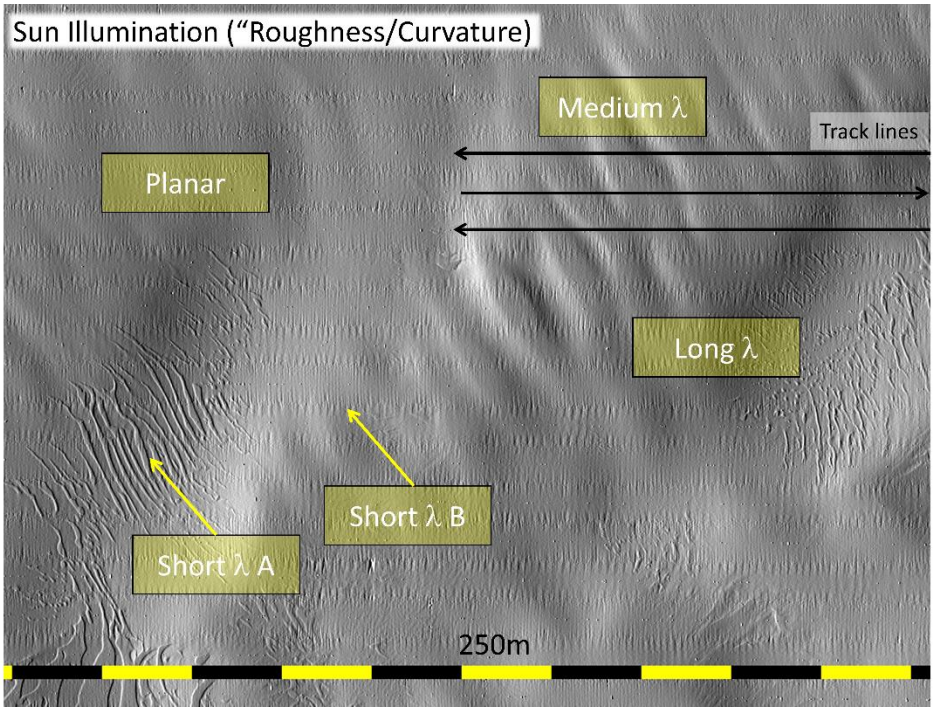

Figure 17: Region of seafloor seeing rapid evolution in seafloor complexity as well as independent, often overlapping undulations, over a spectrum of wavelengths. There is a desire for calibration to be robust to such natural complexity, thus expanding the availability of suitable seafloors.

3.2.3 – Local and Asymptotic Implementation of the RISC

Finally, the RISC approach operates by seeking parameter sets that minimize the mismatch between the wobbled soundings and the smooth quadratic surface. The coupling of the integration errors requires that any optimization scheme for this must be nonlinear. A simple unweighted, iterative least squares adjustment is carried out here, though more sophisticated methods are typical in field implementation ([24], [26], [30], [31], [32], [33]).

A generalized smoothing approach is undertaken, similar to a multivariate implementation of locally weighted scatterplot smoothing (LOWESS), where low-order polynomials, such as the

quadratic surface considered here, are common ([37], [38]). Smoothing is time based, thereby being implemented along-track and lending itself to near-real-time implementation. As discussed previously, a window length twice that of the wobble wavelength will filter half the power of its signature [36]. Further increasing window length ensures the wobbles are increasingly omitted from the surface and free to be allocated to their causal integration errors. A window four times as long as the projected wobble has been found suitable [2], ignoring significantly more than half the power of the wobble's bathymetric signature, though implicitly increases the minimum seafloor wavelength effectively filtered and thus suitable for analysis.

For example, in shallow water conditions, considering a typical wobble wavelength of 40 m projected along-track, a 160 m window is expected to suitably retain the wobble, simultaneously defining the along-track seafloor wavelength which would be suitably filtered to be 640 m. While such an extent is expected to contain tens of thousands of soundings in shallow water conditions, where the seafloor, and thus the propagated integration errors, are heavily sampled, because sounding density decreases as water depth increases, a longer window may be necessary at greater depths.

Notably, at depth, the wobble begins to evolve across-track, as a result of extended shot-receive periods. The across-track window length is here naturally limited to swath width. Assuming a flat seafloor, a swath width is approximately four times the water depth with a $\pm 65°$ swath, or two kilometers in 500 m of water. This ensures the across-track component of the wobbles are suitably ignored by the filter, though increases the potential for their correlation with across-track seafloor undulation, or more specifically, remnant trend. Such artificial correlation causes biased results. Remnant across-track trends are expected to more strongly correlate with the errors that propagate as across-track tilts (errors 3 to 6, page 28). Such artificial correlation generally biases

results. Consequently, across-track undulations far greater than twice the across-track window length, or swath width, are recommended.

While an integration error estimate can be achieved within a single domain, repeating this over successively offset sections of swath corridor adds information to the system, typically increasing accuracy and confidence levels. This is achieved simply through removing the most lagged ping in the current domain and appending the ping which leads it, after each local iterative least squares adjustment. This approach provides a series of smoothed error estimates, which are added to a growing, increasingly asymptotic average. This acts as regional smoothing, having a length scale which grows with time, and thus effectively becomes an asymptotic approach.

This smoothed "monitoring" of each error is particularly useful for parameters which may slowly drift spatiotemporally, such as surface sound speed bias. While the asymptotic average may be inappropriate in such a case, a regional smoothing period for such nonstationary errors should rather be short relative to their drift rate, but long enough to converge to the true value.

In general, a significant number of soundings distributed over multiple phases of motion are desired. This is due to the similarities among the integration error's input-depth relationships for a single orientation instance, which causes ambiguity in determining the signal's source. This ambiguity results in the parameter estimates compensating for each other at each regression iteration, and the estimate converged on by optimization is not necessarily the true solution for the system. Nonetheless, it is one which minimizes the depth residuals in some sense, referred to as spurious, or nonsense regression [39]. This is explored in Chapter 4.3. Soundings acquired when there is no vessel motion are of course no use to analysis, and Chapter 4.3 also demonstrates how various combinations of vessel orientation, in addition to seafloor misfit,

causes local estimates to “walk” about the true value. While a sufficient number of suitable soundings may not be acquired in a single domain, the increasingly asymptotic, regional domain may attain this, assuming parameter values do not change before a stable convergence can be reached.

Notably, sounding independence increases significantly with depth, and typically so does estimate accuracy for a given number of soundings. The total number of independent soundings over a given spatial extent, however, will not exceed the highly-sampled seafloor in shallow waters, and the expectation is that neither do estimate accuracies. With thousands of soundings collected every minute, approaching the order of tens of thousands in shallow water, there is no lack of data for analysis. Whether it is suitable for the method presented here, however, is addressed in the discussion.

IV – RESULTS AND DISCUSSION

This section seeks to identify the method's limitations as a function of first seafloor depth and horizontal wavelength, and then as combinations of component vessel motion frequencies. Swath corridors simulated using real angular motion and heave input are implemented to establish suitability of local and regional domain extents for a number of seafloor depths and wavelengths. Herein, local refers to a particular along-track section of swath corridor, whereas regional refers to the extent over which the asymptotic average is accumulated. A detailed analysis of vessel motion follows, using the temporally parametrized component orientations presented in Chapter 1.3.2, and the seafloor wavelengths which will be identified as suitable in Chapter 4.1, relative to a window length of four wave periods, found suitable for wobble analysis [2]. Each case presented implements six simultaneously forced errors to assess the method's capability when all are superimposed.

It is worth noting that the low frequency trends remaining from misfit of the quadratic surface to the undulating seafloor are of particular significance to this analysis. A sinusoidal surface undulating along-track provides clear, continuous variation in seafloor suitability relative to a quadratic surface, specifically by the resulting rate of change in seafloor slope and curvature over the domain. Analyzing various undulation wavelengths proved useful in assessing the method's ability to operate in non-ideal seafloor environments.

The advantage in the method not requiring specific pairings of overlapping swaths is that the enormous amount of multibeam data typically acquired during mapping missions, and during their transits, may be considered for analysis. There are however regions of seafloor where a suitable reference surface cannot be established by a quadratic, and thus should not be

considered for calibration. This thesis does not seek to identify particular soundings most useful for analysis, but rather to identify suitable characteristic seafloors and vessel motion. As a result, all soundings are considered for final estimates. The analysis implements a swath corridor simulated for approximately eight minutes, or a few kilometers, over a sinusoid oscillating along-track, acquiring on the order of one million soundings in shallow water, here 50 m. Sounding density naturally decreases with depth, the impact of which will be investigated here. Nonetheless, for each of the cases presented here, sounding densities are such that results asymptotically converge to their true values. Further, the time required for suitable convergence will be discussed here in an effort to establish lower limits on seafloor wavelengths suitable for analysis.

Presented results use stochastically perfect input time series, containing only systematic error. The parameter estimate accuracies achieved then represent the geometry of optimization and are not representative of their real world values which also contain, at a minimum, sensor noise. Parameter estimate uncertainties are not rigorously explored here, which requires consideration of input uncertainties, dependence among the parameters and dependence of the input measures through time. A general expectation in regression is improved model geometry, that is to say the georeference and seafloor models better represent reality, in addition to better sampling of the system's input space, achieved by analyzing soundings acquired over various phases of vessel orientation, respectively produce more accurate and robust results.

4.1 – Asymptotically Mitigating Bias

The following table presents the asymptotic average and its 99% confidence interval for 300 m and 500 m seafloor wavelengths at 500 m water depth, as well as for a planar seafloor. Each result employs identical, real motion time series as input. These are repeated for regional depths

of 50 and 5000 m, with every dataset acquired using the same, real motion time series input. These datasets are selected to aid discussion of the various sources of estimate bias observed as a result of increased sounding density and seafloor model accuracy under known vessel motion conditions. True error magnitudes are indicated below their respective column headers. Window lengths are four wave periods in each case, equating to 160m along-track. A minimum domain length of two pings is defined in deep water, as a single shot-receive cycle (around 16 seconds in 5km water) may exceed time domains defined as functions of short wave periods. Error magnitudes are such that they all propagate with peak amplitude of $\pm 0.25\%$ water depth when driven by three degree, eight second sinusoids, as determined through simulation (Fig. 12). Lever arms errors, which are translational and do not scale with depth, are necessarily increased by an order of magnitude in correspondence with each order of magnitude increase in depth, to maintain this 0.25% relative error magnitude.

Table 1: Simulated results of simultaneously present integration errors when driven by time series of real motion illustrated in Figure 12 and acquired over the described seafloor models. Results are typically more accurate in shallow water conditions where the samples over a given window length, here four wave periods, are increased.

Z (m)	λ (m)	ΔL_x -1, -10, -100 m		ΔL_y -1, -10, -100 m		Δt -0.020 s		$\Delta \rho$ 0.02		$\Delta \kappa$ 2°		ΔSSS 5 m/s	
		μ	σ_μ	μ	σ_μ	μ	σ_μ	μ	σ_μ	μ	σ_μ	μ	σ_μ
50	None	-0.997	0.014	-1.000	0.011	-0.020	0.000	0.020	0.000	1.999	0.013	5.044	0.013
	300	-1.132	0.447	-1.154	0.376	-0.020	0.002	0.015	0.007	2.033	0.099	6.356	2.395
	500	-0.985	0.109	-1.020	0.138	-0.020	0.001	0.020	0.001	1.989	0.020	5.075	0.306
500	None	-9.938	0.314	-10.000	0.032	-0.020	0.000	0.020	0.000	1.999	0.003	4.968	0.020
	300	-11.328	3.443	-10.759	1.139	-0.021	0.001	0.021	0.001	1.941	0.271	4.774	0.486
	500	-9.739	1.149	-10.139	0.423	-0.020	0.001	0.020	0.000	1.987	0.039	5.072	0.106
5000	None	-104.00	4.073	-98.750	2.025	-0.020	0.000	0.020	0.000	1.997	0.003	5.013	0.047
	300	-148.73	72.488	-94.391	20.409	-0.019	0.003	0.013	0.005	1.944	0.048	6.167	1.087
	500	-107.00	24.161	-101.49	9.074	-0.018	0.003	0.022	0.014	2.020	0.173	5.134	2.227

As is the general case in regression, the more useful independent information considered in the domain, the more accurate the results. In deep water conditions, reduced point density is a severely limiting factor for the number of soundings available in regression when combined with limited window lengths. This may be adequately balanced, however, by the independence of the soundings, as the motion evolves significantly over the extended ping periods. Further, abyssal plains are common features in the deep ocean, where undulations only over enormous wavelengths, on the scale of tens of kilometers, are expected and thus window extent may be significantly increased over such bathymetry.

Typically, as a result of simply having more information in the same temporal and spatial extents, the shallow water accuracies under identical conditions of vessel motion are usually best. Notable exceptions are a consequence of poor model geometry, induced by both the combinations of component orientations and seafloor misfit.

Seafloor regions which poorly fit the quadratic surface see the unfiltered seafloor trends producing false depth misclosure estimates. The integration errors combine to best minimize the quadratic-relative seafloor misfit. This is expected to generally impose varying degrees of bias on the error estimates, by causing a false, or spurious relationship, typical in time series ([39], [40]).

In the presence of too short an along-track seafloor undulation, the along-track, or x-lever arm error, converges to a biased estimate. This is a result of the remnant unfiltered seafloor, here an along-track undulation, correlating strongest with the resulting x-lever's depth errors, which migrate along-track during adjustment with the static component of the integration error.

For shallow water environments, the SSS and motion scaling error are both biased, and later figures will illustrate their correlation through time. This correlation is confirmed by the least squares covariance matrix, and is attributed to the across-track nonlinearity in the SSS induced depth errors not becoming significantly different from the linear across-track nature of the roll scaling induced depth errors over the short slant ranges occurring in 50 m of water.

Notably, [33] implements *a priori* weighting of parameters, which may see useful extension here. For example, by considering existing knowledge of the ocean environment stability, INS age and lever arm accuracies in allocating the parameters' freedom in adjustment. Further, more sophisticated stochastic models could better account for the correlations and variances expected and observed in datasets, and are recommended for field implementation.

4.2 – Suitable Domain Extent

With the periodicity of open-ocean wind-driven gravity waves being in the spectrum of one and twenty-five seconds ([41], [42]), having most of their power between four and twelve seconds, the motion-dependent, propagated integration errors projected on the seafloor are similarly periodic [2]. As discussed in Chapter 3.2.3, the lower limit on suitable window length is just greater than two wave periods, such that the projected wobbles are adequately excluded from the quadratic surface. Implementing this limit on the window length ensures the true underlying long wavelength seafloor signature is filtered as strongly as possible, at least along track. The consequence of such a temporally short window, however, is less variation in the vessel's component orientation phase over the domain, and thus less independent information, or a reduced sampling of the input space, is available for local regression. The result is that ambiguities between and even among combinations of integration errors can be more severe. For

example, the likelihood of having combinations of roll and pitch which distinguish x and y-lever arm errors decreases; this is explored further in Chapter 4.3. Thus, a suitable window extent of four wave periods is implemented throughout this analysis.

The real motion time series used here to simulate swath corridors is observed to have significant energy in the roll between periods of five and ten seconds, with a definitive peak around 6.5 seconds. Raw spectrums were ensemble averaged in 60 second segments. The pitch time series, on the other hand is somewhat more broadband, also observing higher frequency, lower amplitude oscillation, with a notable peak observed near a five second period (Fig. 18). Considering roll to be generally more significant to analysis, the eight second peak is assigned as the characteristic wave period, and the four wave period window implemented is equivalent to 32 s, or 160 m along-track for a vessel steaming at 5 m/s. Again, the across-track window length naturally averages around four times the regional water depth, which is varied in this analysis.

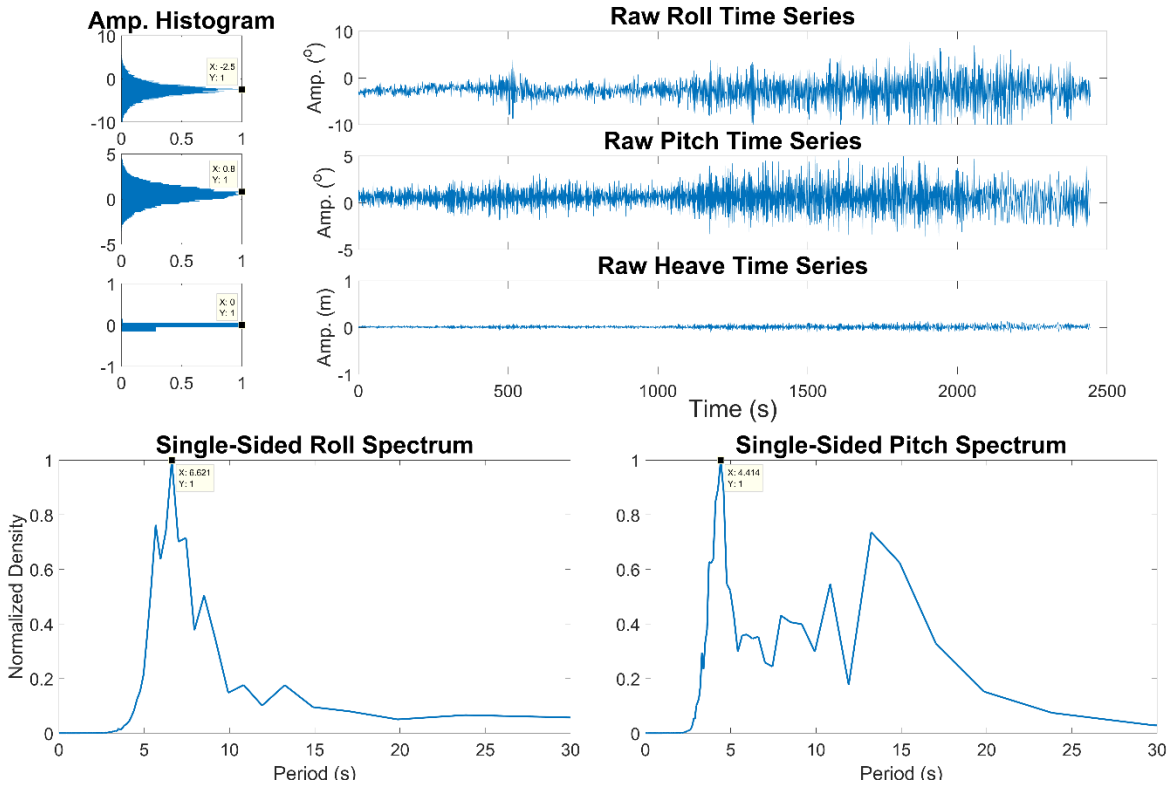

Figure 18: Ensemble-averaged spectrum of the raw, high frequency a) roll and b) pitch time series (window = 60s). Natural motion is observed to be fairly broadband, though clear peaks are distinguishable, here around 6.5 and 4.5 seconds for the roll and pitch components respectively. There is a clear time dependence to the spectrum, resulting from a perceived change in wave conditions when the vessel turns around near the 1000s mark.

Utilizing this real motion time series, obtained from a 10m survey launch, and defining the seafloor's along-track undulation to have a maximum slope of approximately three degrees (a typical limit on natural unconsolidated fine sediments' angle of repose), integration error estimates are presented for a number of synthetic seafloors different depths and along-track wavelengths. This is to determine the method's capability in various seafloor "environments" of interest. The maximum slope is defined analytically through the maximized argument of the sinusoidal surface's along-track derivative:

$$\max\frac{dz}{dx} = \max\left(\frac{d}{dx}\left(A\sin\frac{2\pi x}{L}\right)\right) = \frac{2\pi A}{L}\cdot 1\,rad = \frac{2\pi A}{L}\cdot\frac{180}{\pi}\,deg,$$

having an amplitude-to-wavelength aspect ratio of 0.05.

Figure 19 presents two sequentially-offset local quadratics fit to a 300 m seafloor undulation using a 160 m, or four wave period, along-track window length. While the window length is expected to suitably ignore the high frequency wobbles, it is a bit too long to effectively portray the undulating seafloor. The result is that integration errors (bottom row) as well as the respective adjusted depth misclosures (top middle) are initially grossly inaccurate, apart from motion scaling. Each other estimate is observed to have more than ten percent relative error. This initial result (red surface and value in plots), however, is only the first local estimate and, as the methodology may be repeated sequentially, successive estimates may contribute to an increasingly asymptotic average. Assuming all data to be suitable for analysis, twenty further successively offset local regressions are computer over the next 40 seconds with thus widely different instantaneous orientation combinations and quality of quadratic surface fit. By compiling the running average of the 20, the asymptotic estimate (black surface and value in plots) converges in each case, apart from surface sound speed. The lever arm errors are found to converge dramatically while the surface sound speed diverges by less than 10% relative error. Confidence intervals are here defined

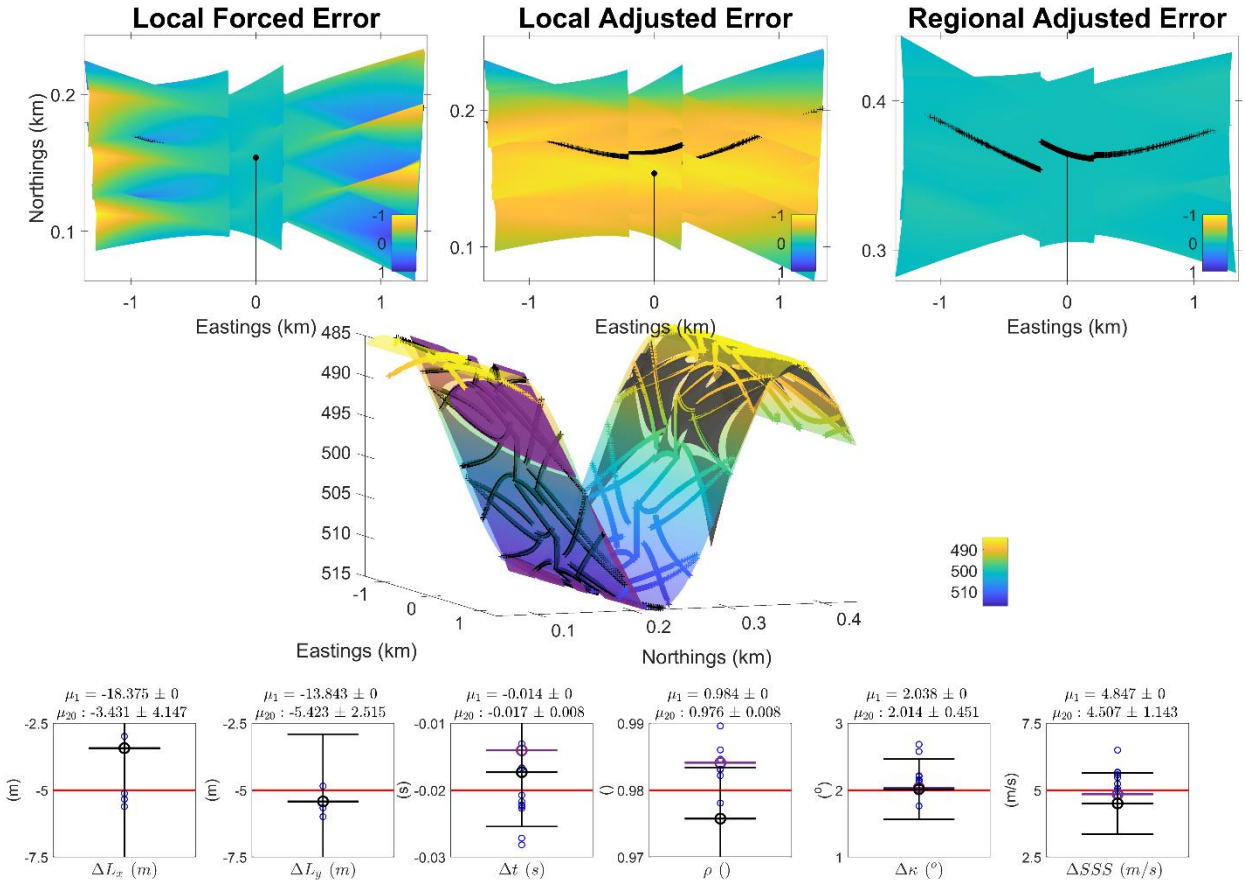

Figure 19: Accuracy of asymptotic integration errors (boxplots, bottom) and quadratic fit estimated using: 1 versus 20 local domains for the regional asymptotic average (red and black bars in boxplots, respectively). The respective surface fits are similarly colored. Blue circles represent each local estimate. The swath corridor is simulated over gently rolling bathymetry, a sinusoid oscillating along-track ($A = 15m, \lambda = 300m, \theta_{max} = 2.86^o$). *Boxplot limits are* $\pm$*50% relative error*

As Figure 19 demonstrates, estimates converge significantly for this medium depth case over the short, 40 s domain presented. The remaining estimates are observed to "walk" a fair amount between successive estimates, though seemingly centered about the true values, in red. This is indicative that analyzing more data may assist convergence. Confidence intervals are defined here assuming each successive average to be an independent draw from the population's distribution, and is therefore undefined for the first estimate. This is a significant simplification, as each successive estimate shares the majority of soundings within the adjacent domains. The result is that uncertainties, and thus confidence intervals, are significantly underestimated.

Nonetheless, this measure of uncertainty is expected to be more realistic than that calculated from the local domain, as presented in Figure 16. An alpha level of 99% is implemented to crudely magnify values as a result of the input dependence inherent in the time series. Consideration of measurement and parameter independence in adjustment and defining confidence is left for future work.

Implementing more data for analysis is highly feasible, as the analysis can be theoretically carried out on all suitable data acquired for mission, and during transit. The following questions are raised:

1) What data is suitable,
2) How much suitable data is required?

Only suitable conditions are presented here, that is, those producing solutions with stable convergence. In order to reduce the computational expense of the method to reasonable magnitudes, however, a data selection scheme should be developed to enable opportunistically analysis of the data most suitable for calibration, similar to [2]. This is expected to aid on the fly (OTF) implementation. Suitability is then defined by how long it takes to reach satisfactory solution convergence. Seafloor and vessel motion suitability are explored through adjusting the input of the swath simulator described in Chapter 1.3.2. The simulated results are free of input uncertainty, and errors here are attributed entirely to system bias. Requirements for effective solution here are then, more specifically, how long until:

1) the parameters are regionally over-identified by a satisfactory number of dependent observations,

2) the bias in the system, here induced by the combination of component vessel orientations, and the variation in seafloor trends occurring within the domain, cancels out.

Figure 20a presents the increasingly asymptotic time series of the locally and regionally smoothed estimates for the above 300 m wavelength case, while Figure 20b presents the results acquired over a slightly longer 500 m along-track section, closer to the 640 m recommended in Chapter 2.3. The y-axis limits presented for each time series are the 99% confidence intervals of each final regional mean for the 300 m dataset, in order to enhance comparison of the two cases. This statistic is calculated assuming each successive average to be an independent draw from the population's distribution. This is a significant simplification, as each successive estimate shares the majority of soundings within the adjacent domains. The result is that uncertainties are significantly underestimated, and confidences are exaggerated. Consideration of measurement and parameter independence in adjustment is left for future work. The figure shows that for an along-track wavelength of 300 m, the asymptotic mean (green line) of the local estimates (blue line) converges to the truth (black line) within approximately three minutes for each error.

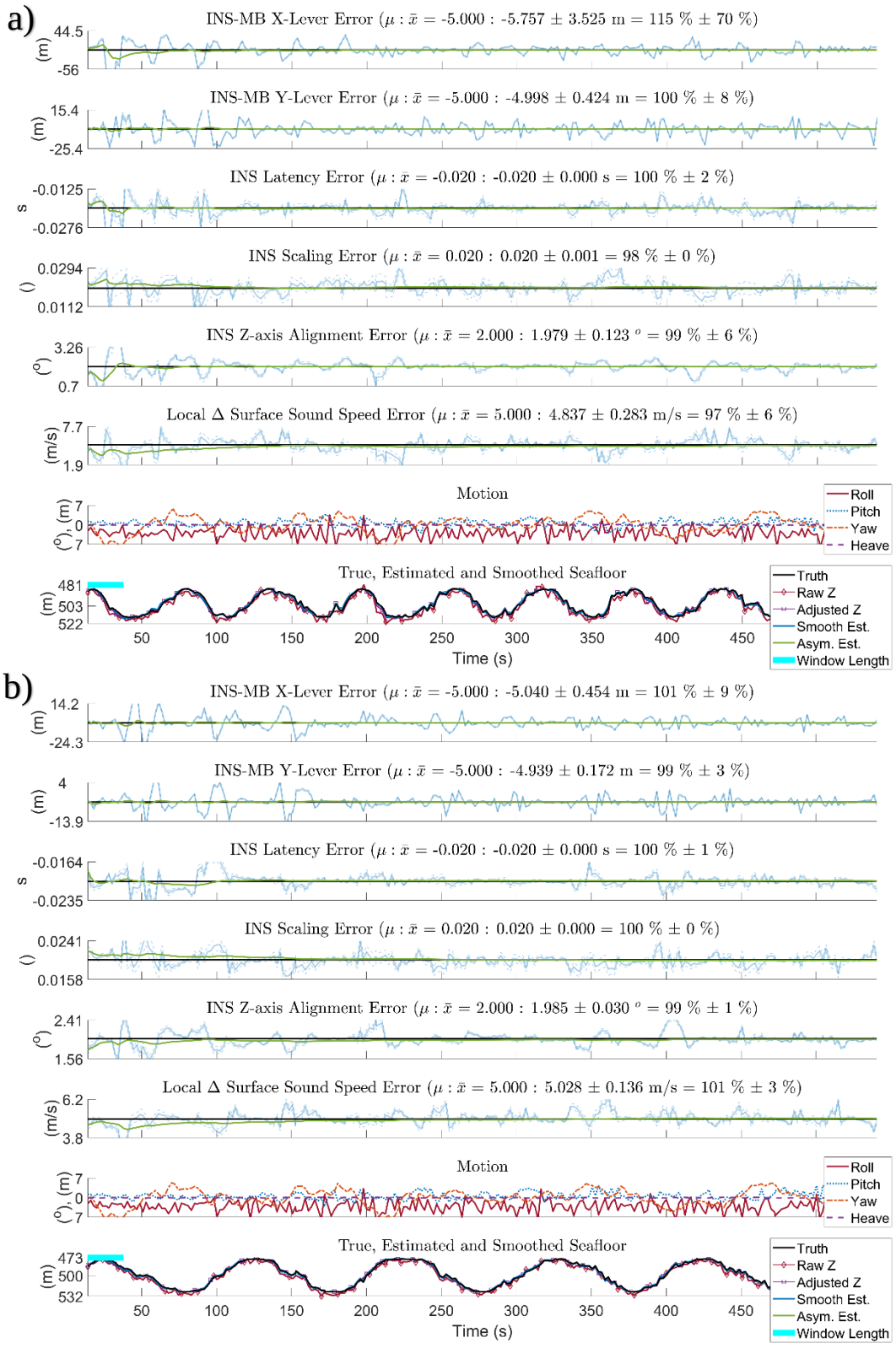

Figure 20: Asymptotic time series of smoothed, local parameter estimates (blue line), their instantaneous asymptotic average (green line) and their true values (black line) for the case of soundings acquired from a platform driven with real motion, over a 500m deep synthetic seafloor, having along-track undulation of a) 300m b) 500m.

As illustrated in Figure 20, initial estimates are highly inaccurate, however, the asymptotic averages are observed to converge to around 10 % and 1% relative accuracies within approximately three minutes for the 300 m and 500 m cases respectively. The results associated with the 500 m along-track are far more favorable, as expected. This is directly a result of consistently better seafloor fits removing more of the true seafloor trend. The seafloor trend not absorbed by the quadratic fit is jointly optimized with the true overprinted wobble, by the integration error's parameters. This biases results if the remaining bathymetric trends are found to spuriously correlate with the propagated errors. This correlation depends on how similar the expected bathymetric characteristics of the sampled wobble is to that of the natural seafloor undulation.

Outside of a simulated environment, imperfect estimates are expected. Further, ambiguities resulting from non-ideal platform motion may arise, also causing the estimates to "walk" about the true values. "Tuning" of the estimates is thus recommended, through analyzing additional local domains, or sections of swath corridor. While estimates for the 500 m case converge to accuracies similar to the 300 m case almost instantly, on closer inspection stable convergence to a significantly increased estimate accuracy similarly occurs at around three minutes, indicating the influence the input motion plays in convergence.

The results demonstrate that consistent along-track undulations having wavelength greater than 300 m and a maximum slope around 3° should be suitable for analysis, once datasets of suitable extent, here approximately three minutes, are acquired. As the regional domain grows through successive local estimates, acquired only from the growing corridor, the imperfect local estimates contribute to an increasingly accurate asymptotic average.

4.3 – Suitable Vessel Motion

With suitable seafloor characteristics identified using typical vessel motion input, the system's response to characteristic component angular velocities of the survey platform motion is investigated, using those surfaces, in order to distinguish the impact of platform motion from that of seafloor misfit.

Wave period is not varied between the expected spectrum of 1 s and 25 s for this section of the analysis, as increased rates only act to increase the magnitude of latency errors. While the vessel goes through more phases of orientation in a given time period, considering characteristic component angular velocities, the rate at which the input space is sampled does not necessarily increase, and is instead depth dependent. Rather, it is the relationships among the various component orientation magnitudes throughout the local, four wave period domain that are of interest for deriving an accurate solution in a given bathymetric environment.

Failure of the method due to vessel motion is only likely to arise when the wave induced platform motion sees extended periods of similar absolute motion magnitudes for roll and pitch, the primary drivers behind each integration error's wobbles. While component oscillation frequencies may be extremely poor for very short periods, considering four wave periods of motion for each local estimate should provide ample time for more suitable combinations to arise. Nonetheless, automatic identification of domains with suitable vessel motion is recommended for future work, particularly for low sea state environments.

In order to analyze the suitability of various combinations of vessel motion, component orientations are simulated here using sinusoids oscillating with deliberately slight offsets in period. This results in the component motions continuously "walking by" each other in phase,

yet never being exactly identical. This motion is then induced over a seafloor with a 500 m along-track wavelength. This produces datasets containing a spectrum of motion and seafloor suitability (Fig. 21), which are the primary drivers behind the method's success. By monitoring the local estimate variations as a function of undulation phase, it is apparent that the quadratic fit is improved at the crests and troughs (where only one inflexion is present), and is worst on the sloped regions where the rate of change of curvature is highest. As long as the misfit estimates are randomly, or more generally, symmetrically distributed, the asymptotic average will converge on the truth, assisted by the more stable solutions.

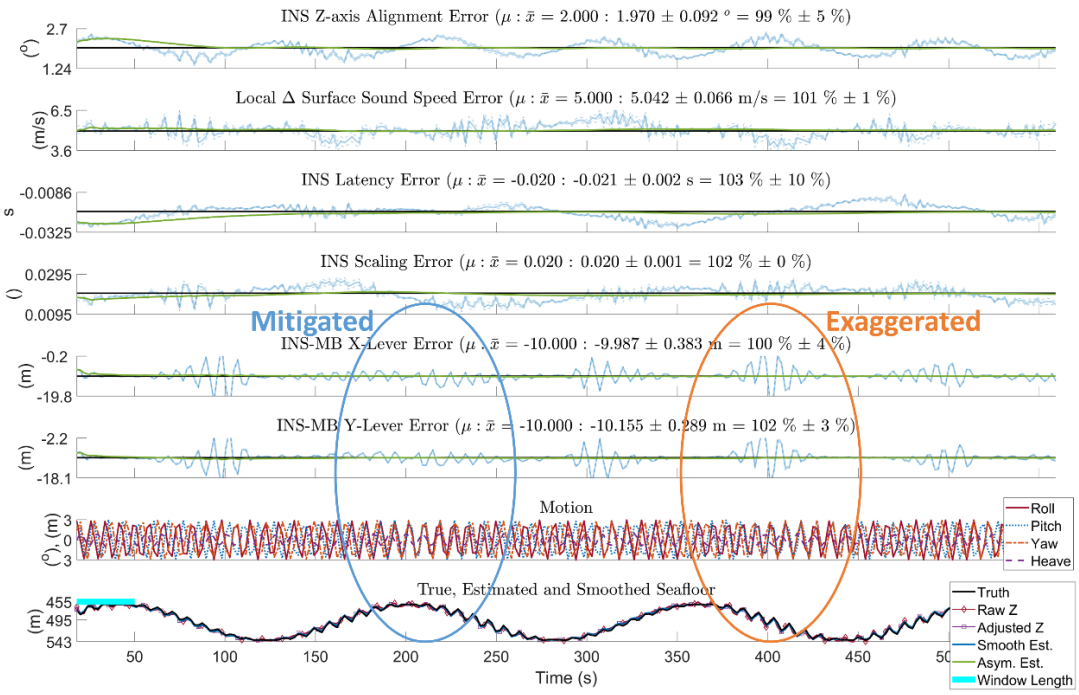

Figure 21: Time series of local estimates driven by synthetic motion such that the vessel component orientations "walk by" each other in phase, oscillating in and out of multicollinearity. This is conveniently aligned with regions of strong and weak seafloor fits, which sees exaggeration and mitigation of spurious regression respectively. This a result of two issues aligning, 1) a roll-pitch induced multicollinearity and 2) a poor seafloor fit.

Periods of extreme uncertainty arise throughout the "monitoring" of the local parameters estimates, with shocks (Fig. 21, lassoed regions) induced by near multicollinearity of the x-lever and y-lever arm errors, and exacerbated by poor seafloor fit. The spurious estimates resulting

from these periods of motion multicollinearity are typically more biased than in the case of seafloor misfit, as the correlation and resulting ambiguity is more severe. This fleeting multicollinearity, occurring when platform roll and pitch are both in phase, as well as when they are out of phase, imposes significant "spikes" on the time series of local lever arm estimates, though does not extend to the sources of angular errors (errors 3 to 6, page 28). In contrast, the angular errors are observed to be more impacted by quadratic surface misfit. Because both the motion multicollinearity and seafloor quadratic misfits are symmetrically distributed over longer time scales, the asymptotic mean is fairly stable through time. This is despite significant variance in the local estimates.

Further, analysis of a simulation driven with identical vessel motion, but forced instead over a flat (Fig. 22a) and long wavelength surface (Fig. 22b), helps to distinguish the impact of wobble-induced misfit, and misfit of the true underlying seafloor. For a flat seafloor, the undulations are observed to have a bias which oscillates with wavelength similar to the window length. This bias results from the quadratic surface fitting a non-integer, or asymmetric sample of wobbles, with the window "following" the wobbles' predominantly along-track undulation. This first bias is found to be significant, and on the order of that resulting from a second source, seafloor misfit. A second "walk" in bias is clearly observed to overlap the first walk in the case of the angular error sources (errors 3 to 6, page 28) in Figure 22b, occurring with a wavelength reflecting that of the true bathymetry. Again, as roll and pitch progressively become in and out of phase, the x and y-lever arm errors become ambiguous, correlating with themselves and compensating for each other in regression. This is the third source of bias observed in the presented system, particularly dominating both lever arm estimate series. Each results in a time-varying spurious bias.

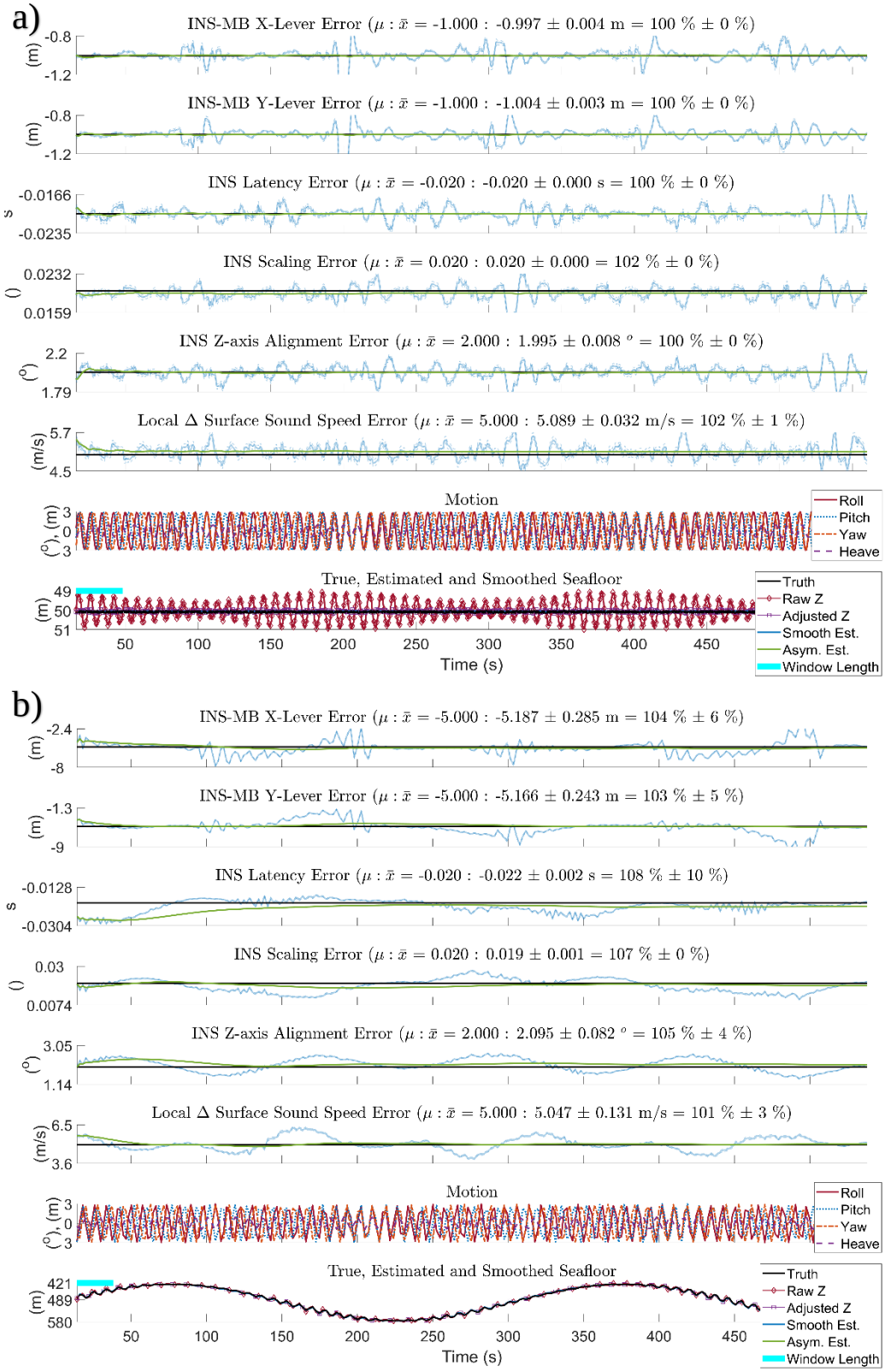

Figure 22: Asymptotic results for identical driving mechanisms used in simulating the dataset presented in Figure 21, when streaming over a) a planar seafloor at 500m, b) a seafloor centered at 500m depth, undulating along-track with 1500m wavelength and a maximum slope of 2.8 degrees.

4.4 – Three Ways to Walk

The time series of the local, smoothed estimates have been shown to "walk", or have a bias which oscillates about their true values. There exist three predominant sources, herein "types", of walk which have been observed in this analysis:

1) the quadratic surface misfits the true seafloor, and an underlying seafloor trend remains, which correlates with the integration errors
2) the quadratic surface is biased by spanning a non-integer number of symmetric wobble oscillations, directly correlating with integration errors,
3) the system input, predominantly the combinations of vessel orientation, or lack thereof, inhibit unique identification of dependent misclosures which resulting from various integration errors.

Repeat estimates from local domains made continuously along-track, over non-ideal seafloor, demonstrates the power of the volume of data acquired by the multibeam in being able to mitigate the impacts of these walks.

Particularly accurate estimates are made when periods of favorable vessel motion and regions of more suitable seafloor fits are progressively steamed over, here the sinusoid's peaks and troughs, where its curvature varies slowest. These accurate local estimates aid convergence of the regional, asymptotic average to the truth. Further, the symmetric nature of the quadratic surface misfits resulting from both superimposed wobbles and real low frequency trends, a result of being designed as sinusoids, are expected to have a zero mean long-term average. This, in combination with the fact that roll-pitch cross correlation is expected to be fleeting, assures

convergence once sufficient data is considered. Thus, even an imperfect estimate of the corridor shape has value, once multiple rolling estimates are combined.

Notably, while high spatial frequency sand waves or rock ridges may have a signature with periodicity similar to some of the wobbles, they are not usually expected to align with the ship track, nor be in phase with the projected motion wavelengths for significant spatial extents. As a result, the asymptotic estimate provided here should, in a limiting sense, be robust to steaming over such high frequency features periodically amongst the generally low frequency, sedimented seafloors found in nature. This assumes the spectrum of the bias through time to approach that of white noise over the increasingly asymptotic regional domain. Despite this, data selection schemes to detect and ignore rough terrains are recommended for efficiency.

The compelling conclusion is that any combination of motion over the local regressed swath corridor, with length a few tens of seconds, is suitable for contribution to a regional average, which is expected to converge to the true integration error, given the impact of motion multicollinearity and seafloor quadratic misfits are asymptotically mitigated as the regional domain length is increased, and the integration errors themselves remain constant

V – CONCLUSION

This thesis has achieved its goal of simultaneously identifying six common integration errors and mitigating their combined total propagated depth error to <0.1% water depth, in all water depths. The errors were set to magnitudes which propagated as depth errors on the order of 0.25% water depth in each case. This was found possible, using the method presented herein, as a consequence of the high frequency dynamics of propagated errors' resulting from the sonar platform's wave-driven dynamics, in addition to an abundance of mundane bathymetry.

First, a generic sounding georeference model was presented which implemented:

1) a concentric approach to determine the direction, $\mathbf{n}_{geoR}$, and virtual origin, $\mathbf{MB}^{MRF}$, that the received echo of a wide-angled transmission was emitted,
2) a curvilinear approach to trace the acoustic signal through a discretized water column.

Integration error terms were included in this georeference model, as well as two additional variables, s and ϕ_R, producing an augmented georeference model in an analytical form, making it suited for optimization.

Following this, a simulator was constructed around the georeference model through parameterizing all sensor inputs, apart from two-way travel time (TWTT) which cannot be calculated in closed form. A brute force approach was taken to trace the signal along the path, initialized by a concentric, non-orthogonal beam vector, $\mathbf{n}_{geo}$, that numerically intersects a sinusoidal surface. This "initial" TWTT was used to update the temporally parametrized vessel state at reception, and integration iterated until a TWTT was satisfactorily converged. This TWTT was then used to reintegrate the sounding, with known integration error forced onto the

auxiliary inputs transformed to the multibeam. This produces a “wobbled” swath corridor for analysis. The simulator demonstrates the impact of various “environmental” characteristics on the nature of the propagated integration errors, particularly water depth and wave-driven angular platform motion.

With the georeference model and simulator in hand, a least squares approach to investigate integration error estimation was developed. Testing was carried out using swath corridors simulated with a three-sector, yaw-pitch-roll stabilized multibeam sonar, operating in typical open-ocean wave conditions. The simulation was run over undulating seafloor terrains with depths ranging from 50 m to 5000 m, thereby simulating both natural long-wavelength seafloor curvature and the wide range of ping periods relative to the ocean wave periods.

The method works by simultaneously estimating the long wavelength curvature of the seafloor and the integration errors using the in situ soundings acquired along a swath corridor. A quadratic surface is proposed for the seafloor. This requires that the regression be performed over length scales large compared to the wavelength of the imprinted motion-dependent errors, yet short relative to the wavelength of the seafloor undulation, and thereby changes in local seafloor curvature. This ensures the wobbles are suitably retained for analysis, while the seafloor is suitably removed.

Over the analyzed section of swath corridor, 1000 to 100,000 depth residuals relative to the simultaneously estimated soundings solutions are used as input to the least squares estimator, depending on water depth.

Instantaneous estimates appear stable within approximately 10% of their true value almost immediately when real motion time series are used as input to the simulator. Finer accuracy

however, depends on the fit of the seafloor and the magnitude and independence of each integration errors' propagated depth errors, predominantly driven by vessel roll, pitch, yaw and heave. Thus, there are periods when the seafloor curvature is poorly estimated and when there is significant correlation between the driving components.

To circumvent the above limitations, a general smoothing approach, similar to LOWESS is applied, with each local estimate contributing to an increasingly asymptotic, regional estimate. This represents a running compilation of all instantaneous solutions. In this manner the solution converges on the true integration errors within better than 1% for most cases. This occurs within approximately three minutes for the datasets driven by real motion data. The resulting seafloor wobble is correspondingly reduced from typical values of $\pm 0.25\%$ water depth to $< \pm 0.01\%$ water depth for the planar case, with result accuracy generally increasing with longer wavelength seafloor undulations.

VI – RECOMMENDATIONS FOR FUTURE WORK

The work presented here is viewed as a simplified approach to assess the feasibility of the presented method for inter-sensor calibration of swath systems. While this proof of concept is effective in ideal conditions, the approach is by no means efficient, and can be made more robust in the case of fleeting data unsuitability. Further, the method implements assumptions on the transmission's geometry which should be relaxed for field implementation. Following is a list of recommendations to consider for optimizing field data:

- The basic least squares cost function and Gauss-Newton optimization schemes are unlikely to be those best suited to this time dependent problem, and were selected here simply for proof of concept. More sophisticated and robust means of optimization exist and should be implemented for field calibration.

- While consistent estimates of the parameters appears feasible in an asymptotic sense, no attempt has been made to address the uncertainties and abundant correlations among the optimization's inputs, and, within the time series of each. These correlations reduce the independence of datasets, and are here primarily influenced by wave induced vessel motion. Consideration of these correlations is recommended to improve optimization efficiency and accuracy, through stronger weighting of more confident observations. This further produces more realistic uncertainties of the integration error estimates, potentially useful in estimating sounding total propagated uncertainty (TPU).

- Domain suitability is paramount here. This may either be assessed prior to optimization, such as through identifying suitable bathymetry and motion, or after the fact using the estimates' statistical properties. The former may be faster, but likely less reliable, though combination

of the two may prove effective. A sophisticated data selection scheme is desired to discriminate between natural rugosity and wobble at all depths. A directional approach employing wavelet analysis may see useful application here. Identification of the statistical suitability of measures may assist in dynamically defining window extents suitable for subdividing a swath corridor, or individual soundings worth disregarding from local domains.

- Each local domain may be optimized in parallel, as the method requires no information to be passed between them. Doing so will significantly reduce processing time, and is easily implemented in the presented scheme. In addition, the use of quaternions is expected to significantly speed up computation and increase numerical stability, and is recommended in place of rotation matrices.
- Finally, this method should be tested on field data to assess the efficacy of the approach under operational conditions. For this, the georeference model used in optimization should itself be more representative of reality, and a non-concentric cone-cone intersection is recommended.

REFERENCES

[1] J. E. Hughes Clarke, "A Reassessment of Vessel Coordinate Systems: What Is It That We Are Really Aligning?," in *US Hydrographic Conference*, Biloxi, MS, 2003.

[2] J. E. Hughes Clarke, "Dynamic Motion Residuals in Swath Sonar Data : Ironing out the Creases," *International Hydrographic Review,* vol. 4, no. 1, 2003.

[3] J. E. Hughes Clarke, "The Impact of Acoustic Imaging Geometry on the Fidelity of Seabed Bathymetric Models," *Geosciences,* vol. 8, no. 4, 2018.

[4] R. A. Pickrill and B. J. Todd, "The Multiple Roles of Acoustic Mapping in Integrated Ocean Management, Canadian Atlantic Continental Margin," *Ocean & Coastal Management,* vol. 46, no. 6-7, pp. 601-614, 2003.

[5] J. E. Hughes Clarke, L. A. Mayer and D. E. Wells, "Shallow-water imaging multibeam sonars: A new tool for investigating seafloor processes in the coastal zone and on the continental shelf," *Marine Geophysical Researches,* vol. 18, no. 6, pp. 607-629, December 1996.

[6] B. J. Todd and G. B. J. Fader, "Quaternary Geology and Surficial Sediment Processes, Browns Bank, Scotian Shelf, Based on Multibeam Bathymetry," *Marine Geology,* vol. 162, no. 1, pp. 165-214, 12 1999.

[7] M. F. J. Wilson, B. O'Connell, C. Brown, J. C. Guinan and A. J. Grehan, "Multiscale Terrain Analysis of Multibeam Bathymetry Data for Habitat Mapping on the Continental Slope," *Marine Geodesy,* vol. 30, no. 1-2, pp. 3-35, 2007.

[8] C. . J. Brown and P. Blondel, "Developments in the Application of Multibeam Sonar Backscatter for Seafloor Habitat Mapping," *Applied Acoustics,* vol. 70, no. 10, pp. 1242-1247, 2009.

[9] M. Schäfer and C. Zwanzig, "Multibeam Echo Sounders for Naval Applications," *Militärische Anwendungen,* 2016.

[10] B. R. Calder and L. A. Mayer, "Automatic processing of high-rate, high-density multibeam echosounder data," *Geochemistry, Geophysics, Geosystems,* vol. 4, no. 6, 2003.

[11] W. H. Greene, Econometric Analysis, Harlow: Pearson Education Limited, 2018.

[12] E. K. P. Chong and S. H. Zak, An introduction to optimization, New York, N.Y.: Wiley, 2008.

[13] J. Beaudoin, J. Hughes Clarke and J. E. Bartlett, "Application of Surface Sound Speed Measurements in Post-Processing for Multi-Sector Multibeam Echosounders," *International Hydrographic Review,* vol. 5, no. 3-4, 2004.

[14] X. Lurton, An Introduction to Underwater Acoustics, Springer-Verlag Berlin Heidelberg, 2010.

[15] D. Chelton, "Probability Concepts," in *Physical Oceanographic and Atmospheric Data Analysis Course Notes,* College of Oceanic and Atmospheric Sciences, Oregan State University, 2015, pp. 7-50.

[16] D. Chelton, Physical Oceanographic and Atmospheric Data Analysis, Course Notes, College of Oceanic and Atmospheric Sciences, 2015.

[17] J. Diebel, "Representing Attitude: Euler Angles, Unit Quaternions, and Rotation Vectors," Stanford University, Stanford, California, 2006.

[18] T. Simpson, Essays on Several Curious and Useful Subjects, in Speculative and Mix'd Mathematicks, London: J. Nourse, 1740.

[19] J. E. Hughes Clarke, "Investigation of the Residual Roll Artifact Present in Mathew 92-008 EM100 Data," Department of Fisheries and Oceans, Canada, DFO Contract Report FP962-2-6001, 1993.

[20] B. Hillard and T. Rulon, "National Oceanic and Atmospheric Administration HydroChart II System "Patch Test" Manual: Ocean Mapping Section," Office of Charting and Geodetic Services, NOS, 1989.

[21] D. Herlihy, B. Hillard and T. Rulon, "National Oceanic and Atmospheric Administration HydroChart II System "Patch Test" Manual: Ocean Mapping Section," Office of Charting and Geodetic Services, NOS, 1989.

[22] J. A. Hammack, J. E. Hughes Clarke, D. H. Fabre and B. Reed, "Hydrographic Multibeam Processing System (HMPS) Swath Alignment Tool," in *Canadian Hydrographic Conference*, Victoria, 1998.

[23] A. Godin, "The Calibration of Shallow Water Multibeam Echo-Sounding Systems. M.Eng. Report, Department of Geodesy and Geomatics Engineering Technical Report No. 190, University of New Brunswick, Fredericton, New Brunswick, Canada, 182 pp.," 1998.

[24] J. T. Bjorke, "Computation of Calibration Parameters for Multibeam Echo Sounders Using the Least Squares Method," *IEEE Journal of Oceanic Engineering,* vol. 30, no. 4, 2005.

[25] J. Eisenberg, M. Davidson, J. Beaudoin and S. Brodet, "Rethinking the Patch Test for Phase Measuring Bathymetric Sonars," 2011.

[26] N. Seube, S. Levilly and K. de Jong, "Automatic Estimation of Boresight Angles Between IMU and Multi-Beam Echo Sounder Sytems," *Quantitative Monitoring of the Underwater Environment,* 2016.

[27] N. Seube and R. Keyetieu, "Multibeam Echo Sounders-IMU Automatic Boresight Calibration on Natural Surfaces," *Marine Geodesy*, vol. 40, no. 2-3, 2017.

[28] R. Keyetieu, N. Seube, V. Djine, G. Roue, B. Clement and P. Bosser, "Multi-Beam Echo Sounders–INS Automatic Latency Calibration," *Marine Geodesy,* vol. 41, no. 5, 2018.

[29] T. Schenk, "Modeling and Analyzing Systematic Errors in Airborne Laser Scanners," Technical Notes in Photogrammetry No 19; The Ohio State University: Columbus, OH, USA, 2001.

[30] S. Filin, "Recovery of Systematic Biases in Laser Altimetry Data Using Natural Surfaces," *Photogrammetric Engineering & Remote Sensing,* vol. 69, no. 11, 2003.

[31] P. Freiss, "Towards a Rigorous Methodology for Airborne Laser Mapping," Proceedings of the International Calibration and Validation Workshop EURO COW, Castelldefels, Spain, 2006.

[32] J. Skaloud and D. Lichti, "Rigorous Approach to Bore-Sight Self-Calibration in Airborne Laser Scanning," *ISPRS Journal of Photogrammetry and Remote Sensing,* vol. 61, no. 1, 2006.

[33] M. Gonsalves, "A Comprehensive Uncertainty Analysis and Method of Geometric Calibration for a Circular Scanning Airborne Lidar," 2010.

[34] D. Cartwright and J. Hughes Clarke, "Multibeam Surveys on the Fraser River Delta, Coping with an Extreme Refraction Environment," Ocean Mapping Group, Dept. Geodesy and Geomatics Engineering, University of New Brunswick, New Brunswick, 2002.

[35] D. Dinn, B. Loncarevic and G. Costello, "The Effect of Sound Velocity Errors on Multibeam Sonar Depth Accuracy," *Proceedings of the Oceans '95 Conference, Oct. 9 – 12, 1995, San Diego, California, USA,* 1995.

[36] P. D. Willson and S. R. Polo, "Polynomial Filters of Any Degree," *Journal of the Optical Society of America,* vol. 71, no. 5, 1981.

[37] W. S. Cleveland, "Robust Locally Weighted Regression and Smoothing Scatterplots," *Journal of the American Statistical Association,* vol. 74, no. 368, 1979.

[38] W. S. Cleveland and S. J. Devlin, "Locally Weighted Regression: An Approach to Regression Analysis by Local Fitting," *Journal of the American Statistical Association,* vol. 83, no. 403, 1988.

[39] C. W. J. Granger and P. Newbold, "Spurious Regressions in Econometrics," *Journal of Econometrics,* vol. 2, no. 2, 1974.

[40] Z. Wu, N. E. Huang, S. R. Long and C.-K. Peng, "On the trend, detrending, and variability of nonlinear and nonstationary time series," *Proceedings of the National Academy of Sciences,* vol. 104, no. 38, 2007.

[41] L. H. Holthuijsen and C. U. Press, Waves in Oceanic and Coastal Waters, Cambridge University Press, 2015.

[42] A. Toffoli and E. M. Bitner-Gregersen, "Types of Ocean Surface Waves, Wave Classification," *Encyclopedia of Maritime and Offshore Engineering,* 2017.